

Identifying, and constructing, complex magnon band topology

Alberto Corticelli,¹ Roderich Moessner,¹ and Paul A. McClarty¹

¹Max Planck Institute for the Physics of Complex Systems, Nöthnitzer Str. 38, 01187 Dresden, Germany

Magnetically ordered materials tend to support bands of coherent propagating spin wave, or magnon, excitations. Topologically protected surface states of magnons offer a new path towards coherent spin transport for spintronics applications. In this work we explore the variety of topological magnon band structures and provide insight into how to efficiently identify topological magnon bands in materials. We do this by adapting the topological quantum chemistry approach that has used constraints imposed by time reversal and crystalline symmetries to enumerate a large class of topological electronic bands. We show how to identify physically relevant models of gapped magnon band topology by using so-called decomposable elementary band representations, and in turn discuss how to use symmetry data to infer the presence of exotic symmetry enforced nodal topology.

Introduction – There have been considerable efforts in the last few years to provide a taxonomy of nontrivial topological band structures enforced or allowed by time reversal and crystalline symmetries [1–13]. This work has brought powerful new concepts that tie crystal and magnetic structures to band topology. At the same time these ideas provide efficient methods to efficiently search for topological materials resulting in a vast database of *ab initio* driven predictions of new electronic topological materials [14, 15]. Such materials include gapless and gapped bulk topological matter with protected boundary states and anomalous transport properties. The culmination of these efforts to classify band topology based on symmetry and to use symmetry data to diagnose topological bands is called topological quantum chemistry (TQC) [6, 12].

In a similar time frame, there has been increasing interest in exploring the role of band topology in *magnetic* excitations and how it affects the properties of magnetic materials [16–18]. The pioneering work in this area has mainly been in devising physically well-motivated models of magnon band topology such as Chern insulators and Weyl magnons [19–33]. This has inspired early experimental efforts to characterize magnon topology in materials [34–39]. All this work has gone hand-in-hand with the exploration of unusual transport properties in insulating magnets such as the thermal Hall effect [40–48] and the exploration of signatures of bulk nodal magnon topology in neutron scattering experiments [36, 37, 49]. On the horizon, there are exciting potential spintronics developments to be made detecting and manipulating topological magnon boundary states [50–53].

In this paper, we show that the TQC approach can be adapted to magnon band topology, providing a classification of *symmetry-determined* topological bands in spin wave Hamiltonians. The ideas can be used to diagnose magnon topology on one hand, and on the other to build models and identify candidate topological magnon materials. The physical foundation for this work is that topological bands by definition cannot be built from a Wannier basis while preserving all underlying symmetries. Topological quantum chemistry rests on an enumeration

of all possible Wannierizable band structures through so-called elementary band representations (EBRs), to be described in more detail below so that, essentially by elimination, one may establish whether some set of bands is topologically nontrivial.

Ab initio methods are central to TQC. The closest analogue in widespread use to study magnetic excitations is linear spin wave theory which is based on an expansion, to quadratic order, of the spins in fluctuations around some magnetic structure. The goal of this paper is to show how to pass from elementary symmetry information – the crystal structure and the magnetic order – to linear spin wave models with nontrivial topology.

Our starting point is to establish how crystal and time reversal symmetries are implemented within linear spin wave theory. In contrast to electronic systems, the band structures of interest emerge from an effective exchange Hamiltonian. We describe how this Hamiltonian, in conjunction with the minimal energy magnetic structure, fixes the symmetries of the problem. These are encoded in some magnetic space group. We then outline how to build band representations for magnons starting from the local moments on each magnetic site giving a complete table of all site symmetry groups compatible with magnetic order. Band representations minimally encode symmetry information in the magnon band structure. With these ingredients, we are in a position to identify constraints that magnons place on the possible symmetry data and hence on the possible topological bands. In particular, it turns out that magnons in systems with *significant spin-orbit coupling* form a subset of all electronic topological bands.

With these foundations, we then show, first in general and then through a series of examples, how to use symmetry information alone to build exchange models whose elementary excitations have nontrivial gapped and nodal magnon topology and to identify candidate materials. Examples include Chern bands, antiferromagnetic topological insulators, and three-fold and six-fold nodal points. Crucially, our workflow can be straightforwardly reversed, to diagnose nontrivial topology from spin wave fits to experimental data.

EBRs and Topology – Before getting into the specifics for magnons, we give a lightning introductory review of TQC. We refer the reader to the supplementary section [54] for more technical details that will not, however, be necessary to appreciate the remainder of this paper.

The essential symmetry ingredients of TQC are nothing more than the symmetry group G_M of the magnetic structure and the Wyckoff positions of the magnetic ions that appear in any structural refinement of a magnetic material. The group G_M is generally one of the magnetic space groups that encodes combinations of crystallographic point group symmetries, lattice translations, time reversal symmetry and perhaps non-symmorphic elements. To each Wyckoff position \mathbf{q} , we may assign a site symmetry group (SSG) $G_{\mathbf{q}}$ defined as the subgroup of G_M that leaves the site invariant. This is generally isomorphic to a magnetic point group.

We then need to include some information about the underlying lattice degrees of freedom – the nature of the atomic orbitals. These necessarily transform under some representation of $G_{\mathbf{q}}$. Following Zak, from these representations of the magnetic SSG we may arrive at a representation of the full G_M group by the standard process of *induction* [55]. The result is a so-called band representation (BR). The BR is a momentum space representation of all elements of G_M that contains information about the connectivity of the bands and the topology. To connect to topology we define elementary band representations (EBRs) to be BRs that are not unitarily equivalent to a direct sum of two or more BRs. These hold a distinguished place in relation to topology because they are the elementary units from which all Wannierizable band structures can be built for a given symmetry group. Any set of bands that cannot be built from EBRs is necessarily topological overall. All EBRs for all magnetic space groups have been tabulated – each one characterized by eigenvalues of all symmetry operations at high symmetry momenta. For all 1,651 magnetic space groups, there are roughly 20,000 EBRs. In order to diagnose topological bands, one should in principle determine whether each energetically isolated set of bands can be written as a direct sum of EBRs with non-negative integer coefficients. If so, the bands are trivial. If not, they are symmetry-determined topological bands. A more fine-grained determination of the nature of the topology then requires further analysis. Symmetry enforced nodal topological bands can be read off directly from the dimension greater than one irreducible representations at high symmetry points, lines and planes.

Magnons and Symmetry – Building on the principles behind TQC we now discuss the ideas in relation to magnons. In this work we are mainly interested in crystalline solids with localized magnetic moments and non-vanishing local dipolar order parameter $\langle S_i^\alpha \rangle$ for site i and component α . The magnon or spin wave excitations are the transverse fluctuations of the local ordered mo-

ments. We restrict our attention to the typical case where these form coherent propagating bands. This means we neglect the role of multi-magnon states and possible interesting questions of novel topology [56] and fragility that arise from such states. We also neglect magnetic excitations beyond the ground state multiplet that could be handled within a multi-boson formalism (see e.g. [36]) to which TQC ideas may also be applied.

The symmetries of the magnon bands are descended from those of the magnetic Hamiltonian H_M considered to be composed of exchange couplings, dipolar couplings, single ion anisotropies and perhaps an external magnetic field. The magnetic order breaks the symmetries of the magnetic Hamiltonian down to a subgroup. It is important to note that the relevant symmetry groups for magnons are single-valued because the bands are spinless or bosonic. These are the groups that are relevant to weakly spin-orbit coupled electronic systems. However, in the context of magnons, these groups are relevant to the case where the moments and the spatial transformations are locked, which can only happen when spin-orbit coupling at the microscopic level is significant. The spin-orbit coupling is reflected in the appearance of anisotropies in the magnetic Hamiltonian. As is well-known, there are many cases where the magnetic Hamiltonian has discrete or continuous rotation symmetries. In such cases, magnetic order may lead to residual symmetries described by the spin-space groups [57–60]. Topological quantum chemistry applied to such groups is beyond the scope of this work. We consider the case where these residual symmetries are those of a magnetic space group G_M with n_S sublattices in the magnetic primitive cell leading to n_S bands considered to be computed from linear spin wave theory based on Hamiltonian $H_{LSW} = \frac{S}{2} \sum_{\mathbf{k}} \hat{\mathbf{Y}}^\dagger(\mathbf{k}) \mathbf{M}(\mathbf{k}) \hat{\mathbf{Y}}(\mathbf{k})$ where the transformation properties of $2n_S$ component $\hat{\mathbf{Y}}(\mathbf{k})$ can be inferred from the transformations of the S_i^\pm transverse spin components in a frame where S^z is the direction of the ordered moment. For reference, explicit formulas are given in the Supplementary Section [54].

To build band representations, we must first identify the SSG from that of the Wyckoff position of the magnetic ions by requiring that the on-site S^z transforms as the total symmetric irrep of the SSG. This constraint reduces the possible 122 magnetic point groups to a set of 31 groups isomorphic to SSGs. The relevant orbital content is given by the local frame transverse spin components S_i^\pm . We give a complete list of the magnetic SSGs in the Supplementary Section together with the irreducible representations of the SSG for which S_i^\pm form a basis [54].

Given this information, one may build a band representation for magnons and, again, explicit formulas are given in the Reference Material [54]. Given an energetically isolated set of magnon bands one may then ask whether this decomposes into EBRs. The EBRs relevant

to magnons corresponding to all magnetic structures and significant spin-orbit exchange are tabulated. In the remainder of this paper we give concrete examples of how to use the tabulated EBRs to build models of topological magnons. We take two main routes. The first is to focus on cases where the symmetry information about band connectivity allows EBRs to split up into disconnected bands. By definition at least one of the resulting bands must be topological. Our second focus will be on nodal topology. Several models are known with Dirac and Weyl magnon touching points [16]. But symmetry can enforce higher order degeneracies 3, 4 and 6-fold degeneracies, and we show how to build models with such degeneracies.

Magnon topology from decomposable EBRs – To build models of decomposable EBRs we focus on cases where the magnetic ions live on *maximal* Wyckoff positions, i.e. positions of maximal magnetic point group symmetry for a given G_M . These are distinguished by the fact that BRs induced from such sites are themselves EBRs and not composites of EBRs (apart from some well-understood exceptional cases). We give a complete table of decomposable EBRs that can be obtained from maximal Wyckoff positions and the allowed SSGs organized by magnetic space group and Wyckoff position [54]. The utility of this table is that one may couple moments living on such Wyckoff positions and be sure that there will be nontrivial topology in the resulting magnon bands provided free parameters are tuned to avoid accidental degeneracies and provided the number of free parameters is adequate to reduce the symmetries to the required G_M . This approach is a highly efficient means to build models of magnon topology and contrasts to generic cases of nontrivial topology where, in practice, one should compute so-called symmetry indicators as a function of free couplings to diagnose the topology.

We take an example to illustrate the main ideas – the well-established case of Chern magnon bands in the Kitaev-Heisenberg honeycomb model with [111] polarized moments [31, 61]. We reverse the usual logic to show how the model might have been inferred from the tabulated decomposable EBRs. Let us consider magnetic space group $F\bar{3}1m'$ (#162.77 in the BNS convention) and Wyckoff position $2c$ corresponding to honeycomb layers. The magnetic site symmetry group is $32'$ and the moments are perpendicular to the honeycomb planes. The orbital basis on the $2c$ positions ($J_{\mathbf{q}}^+, J_{\mathbf{q}}^-$) transforms under the ${}^1E + {}^2E$ irreps of the SSG. Consultation of tables in the Supplementary Section [54] or on the Bilbao crystallographic server [62, 63] reveals that induction to the full space group yields a single EBR that is decomposable into two bands. From symmetry alone we have therefore inferred the presence of nontrivial magnon band topology. A guide to using the Bilbao tables is given in the Supplementary Section [54].

With this established, we may now build a model host-

ing the decomposable EBR and further characterize the nature of the topology. To do this, one should write down couplings between the magnetic moments that both stabilize the required magnetic structure and respect the resulting magnetic space group symmetries. Both conditions are important. For example, it is straightforward to stabilize the structure with ferromagnetic Heisenberg exchange but the resulting model has higher symmetry than $F\bar{3}1m'$ owing to a spin-space symmetry coming from the spin rotation symmetry of the underlying Hamiltonian. One may systematically compute all exchange couplings allowed by symmetry. To nearest neighbor these are the Heisenberg, Kitaev, Γ and Γ' terms [31, 64]. Kitaev and Heisenberg are sufficient to respect $F\bar{3}1m'$ and a magnetic field may be applied along [111] to stabilize the structure if necessary. A linear spin wave calculation then reveals two propagating magnon bands with a gap between them. For decomposable EBRs the topology is not necessarily symmetry indicated but it turns out that the C_3 symmetry indicator formula [1] for the Chern number characterizes the topology in this case:

$$\exp\left(\frac{2\pi i}{3}C\right) = \prod_n \Theta_n(\Gamma)\Theta_n(K)\Theta_n(K') \quad (1)$$

where the product is over n bands and $\Theta_n(\mathbf{k})$ is the eigenvalue of C_3 at wavevector \mathbf{k} in band n . This reveals that the model has two magnon bands with Chern numbers ± 1 , the order depending on the sign of the Kitaev exchange.

We now sketch another example of gapped band topology working from the table of decomposable EBRs but this time without reference to an example already in the literature. Consider space group $P4$ (#75.1, a type I MSG) with Wyckoff position $2c$ and irreps $2B$ for the transverse spin components. This again leads to a single decomposable EBR, now with SSG C_2 compatible with ferromagnetic [001] magnetic order. The lattice is tetragonal with a basis $(0, 1/2, 0)$ and $(1/2, 0, 0)$. We compute all symmetry-allowed exchange couplings for first up to fourth nearest neighbors and choose some set of couplings that stabilizes the required magnetic structure. The linear spin wave spectrum has two dispersive gapped bands and the Chern number can, once again, be computed from a symmetry indicator formula

$$i^C = \prod_n \xi_n(\Gamma)\xi_n(M)\zeta_n(X) \quad (2)$$

where C is the Chern number of the n band(s), while $\xi(\mathbf{k})$ and $\zeta(\mathbf{k})$ are the eigenvalues respectively of C_4 and C_2 . Fig. 1 shows the lattice structure and the band structure with the eigenvalues indicated. The computed Chern numbers are ± 1 .

The method is not restricted to diagnosing Chern bands as we show now with a third example. We take space group P_6/mcc (#192.252) and Wyckoff position

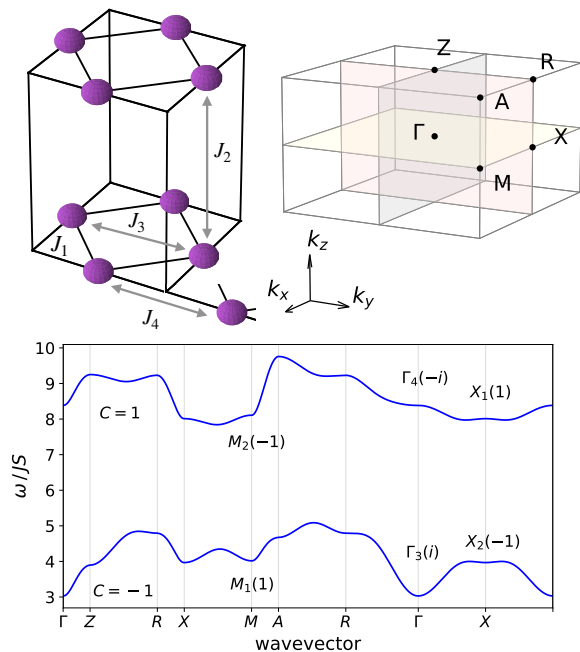


FIG. 1. Figure showing the magnetic sublattices of space group 75 Wyckoff position 2c and the accompanying Brillouin zone. The lower panel shows magnon dispersion relations along high symmetry directions with the C_2 and C_4 eigenvalues given according to the symmetry indicator formula Eq. 2.

4c which has SSG $-6m'2'$. This corresponds to an AA stacked honeycomb lattice with moments perpendicular to the plane that are ferromagnetically ordered in the plane and antiferromagnetically aligned between planes. Crucially this system is symmetric under time reversal times a translation that maps one layer to the next. The two magnon bands within each layer each carry a net Chern number which reverses between layers. One may show [54] that the coupled four magnon bands correspond to a single EBR that is decomposable. The result is an antiferromagnetic topological insulator that can be realized with an anisotropic exchange model for the in-plane moments with Heisenberg exchange between the layers. An explicit calculation of the band structure is provided for reference [54] (see also [65]).

Symmetry enforced nodal topology – In this part, we turn our attention to nodal topology focussing on exotic degeneracies that are enforced by symmetry: magnonic analogues of multifold fermion degeneracies [66, 67]. In the supplementary section we show how to use the Bilbao tables [62, 63] to establish symmetry-enforced degeneracies and give extensive tables of such degeneracies for magnons [54]. Here we show how to build models based on the symmetry information.

The first example is for magnetic space group 227.131 – a type III group – and Wyckoff position 16d corresponding to all-in/all-out (AIAO) order on the A

site of pyrochlore materials as realized in $\text{Nd}_2\text{M}_2\text{O}_7$ ($\text{M}=\text{Sn}, \text{Hf}, \text{Ir}, \text{Zr}$) [68–72], $\text{Sm}_2\text{Ir}_2\text{O}_7$ [73], $\text{Eu}_2\text{Ir}_2\text{O}_7$ [74], $\text{Cd}_2\text{Os}_2\text{O}_7$ [75] as well as FeF_3 [76]. The magnetic structure has a magnetic 2-fold screw and a magnetic S_4 symmetry. The single-valued symmetry group enforces a 3-fold degenerate point at Γ [62, 63]. We may establish this fact directly from a simple model for the magnons consisting of antiferromagnetic Heisenberg coupling with a weak $\langle 111 \rangle$ Ising anisotropy in the exchange that lifts the considerable degeneracy of the Heisenberg model [77] in favor of the AIAO structure. A linear spin wave calculation based on this model [54] reveals four dispersive modes with a spectral gap and the three-fold degenerate point at Γ . The existence of this quadratically dispersing three-fold point has previously been noted in Ref. [78] as a parent state for Weyl fermions upon symmetry breaking with strain or an applied magnetic field.

Our next example has both three-fold and six-fold degenerate magnons. Inspection of the table of degeneracies [54] reveals six-fold degeneracies for magnetic space group 230.148 and Wyckoff position 24c. The nearest neighbor exchange leads to two decoupled magnetic sublattices of corner-sharing triangles. This is the hyperkagome structure that arises on the R sites of garnets with chemical formula $\text{R}_3\text{M}_5\text{O}_{12}$. The magnetic structure compatible with 230.148 is shown in Fig. 2. The moments are oriented along three cubic directions on each triangular face. This structure is observed in the material $\text{Dy}_3\text{M}_5\text{O}_{12}$ ($\text{M}=\text{Al}, \text{Ga}$) [79–81]. The 24 Wyckoff sites are composed of 12 magnetic sublattices plus a translation through $(1/2, 1/2, 1/2)$ as the lattice is bcc. We therefore expect 12 magnon modes. We compute the symmetry-allowed exchange couplings to nearest neighbor. There are six such couplings and one of these is an effective Ising exchange with easy axes along the cubic directions on different sublattices in the pattern required to stabilize the magnetic structure. With this as the dominant coupling, we consider a model with all six nearest neighbor couplings included and with antiferromagnetic Heisenberg exchange coupling the two hyperkagome sublattices. A sample spin wave spectrum is shown in Fig. 2. This has several multi-fold bosonic points including four 3-fold points at Γ with quadratic dispersion and one 6-fold point at H on the zone boundary with linear dispersion that is a doubled spin-1 Weyl point. All the degeneracies in the spectrum are compatible with the group theory analysis.

Discussion – The classification of topological materials based on crystalline and time reversal symmetries is at a mature stage. In the foregoing we have connected the symmetry-based classification scheme based on elementary band representations to topological magnons. To do this, we showed how symmetries are inherited by magnons from those of the underlying exchange Hamiltonian and indicated how to build band representations for magnons. We have given conditions for the ex-

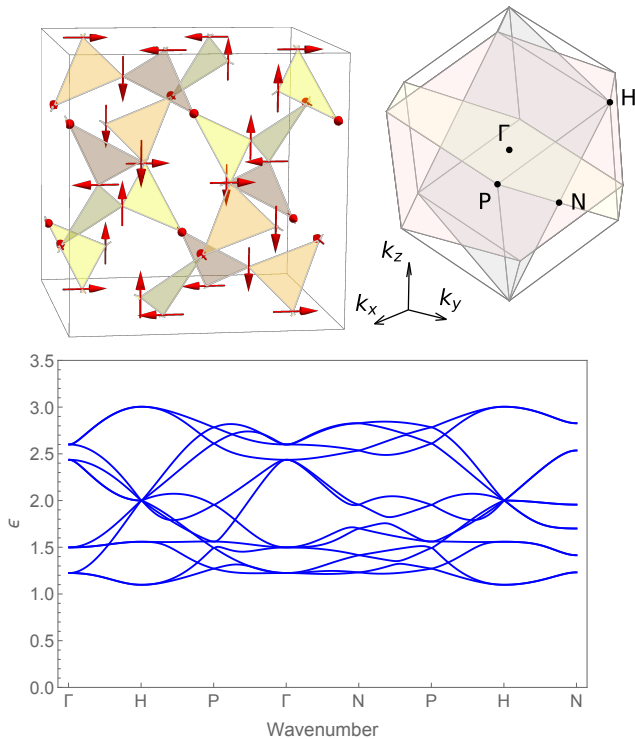


FIG. 2. Magnetic structure on the garnet hyperkagome lattice with 230.148 magnetic space group symmetry (top left) and (right) the Brillouin zone with high symmetry points indicated. Bottom: spin wave spectrum with multi-fold magnons at Γ and H .

isting tables of EBRs to be applicable to topological magnons. We have shown through several examples that one can use the computed decomposable elementary band representations for single-valued magnetic space groups to build realistic, non-fine-tuned models of topological magnon band structures. We have also used tabulated symmetry-enforced degeneracies as a guide to building exchange models of exotic nodal topology such as six-fold degenerate touching points. Magnons provide an excellent platform to explore the interplay of magnetic symmetries and topology in conjunction with inelastic neutron scattering. In addition to model-building and experimental discovery within the framework laid out here, important open avenues are to explore magnon topology beyond the decomposable EBR paradigm within the TQC framework and to extend TQC to the spin-space groups that are applicable to Heisenberg models among other systems.

PM acknowledges useful discussions with Alexei Andreev on magnetism in the garnets. This work was in part supported by the Deutsche Forschungsgemeinschaft under grants SFB 1143 (project-id 247310070) and the cluster of excellence ct.qmat (EXC 2147, project-id 390858490).

- [1] C. Fang, M. J. Gilbert, and B. A. Bernevig, *Physical Review B* **86** (2012), 10.1103/physrevb.86.115112.
- [2] S. A. Parameswaran, A. M. Turner, D. P. Arovas, and A. Vishwanath, *Nature Physics* **9**, 299–303 (2013).
- [3] H. Watanabe, H. C. Po, A. Vishwanath, and M. Zaletel, *Proceedings of the National Academy of Sciences* **112**, 14551–14556 (2015).
- [4] H. C. Po, H. Watanabe, M. P. Zaletel, and A. Vishwanath, *Science Advances* **2** (2016), 10.1126/sciadv.1501782.
- [5] H. Watanabe, H. C. Po, M. P. Zaletel, and A. Vishwanath, *Phys. Rev. Lett.* **117**, 096404 (2016).
- [6] B. Bradlyn, L. Elcoro, J. Cano, M. G. Vergniory, Z. Wang, C. Felser, M. I. Aroyo, and B. A. Bernevig, *Nature* **547**, 298–305 (2017).
- [7] J. Kruthoff, J. de Boer, J. van Wezel, C. L. Kane, and R.-J. Slager, *Phys. Rev. X* **7**, 041069 (2017).
- [8] H. Watanabe, H. C. Po, and A. Vishwanath, *Science Advances* **4** (2018), 10.1126/sciadv.aat8685.
- [9] J. Cano, B. Bradlyn, Z. Wang, L. Elcoro, M. G. Vergniory, C. Felser, M. I. Aroyo, and B. A. Bernevig, *Phys. Rev. B* **97**, 035139 (2018).
- [10] Z. Song, T. Zhang, Z. Fang, and C. Fang, *Nature Communications* **9** (2018), 10.1038/s41467-018-06010-w.
- [11] Z. Song, T. Zhang, and C. Fang, *Phys. Rev. X* **8**, 031069 (2018).
- [12] L. Elcoro, B. J. Wieder, Z. Song, Y. Xu, B. Bradlyn, and B. A. Bernevig, “Magnetic topological quantum chemistry,” (2020), arXiv:2010.00598 [cond-mat.mes-hall].
- [13] Y. Xu, L. Elcoro, Z.-D. Song, B. J. Wieder, M. G. Vergniory, N. Regnault, Y. Chen, C. Felser, and B. A. Bernevig, *Nature* **586**, 702–707 (2020).
- [14] M. G. Vergniory, L. Elcoro, C. Felser, N. Regnault, B. A. Bernevig, and Z. Wang, *Nature (London)* **566**, 480 (2019), arXiv:1807.10271 [cond-mat.mtrl-sci].
- [15] “Topological materials database,” <https://topologicalquantumchemistry.org/>.
- [16] P. A. McClarty, *Annual Review of Condensed Matter Physics* **13** (2022), 10.1146/annurev-conmatphys-031620-104715.
- [17] V. Bonbien, F. Zhuo, A. Salimath, O. Ly, A. About, and A. Manchon, *Journal of Physics D: Applied Physics* **55**, 103002 (2021).
- [18] M. Malki and G. Uhrig, *EPL (Europhysics Letters)* **132**, 20003 (2020).
- [19] L. Zhang, J. Ren, J.-S. Wang, and B. Li, *Phys. Rev. B* **87**, 144101 (2013).
- [20] R. Shindou, J.-i. Ohe, R. Matsumoto, S. Murakami, and E. Saitoh, *Phys. Rev. B* **87**, 174402 (2013).
- [21] R. Shindou, R. Matsumoto, S. Murakami, and J.-i. Ohe, *Physical Review B* **87**, 174427 (2013).
- [22] A. Mook, J. Henk, and I. Mertig, *Phys. Rev. B* **94**, 174444 (2016).
- [23] A. Mook, J. Henk, and I. Mertig, *Phys. Rev. B* **91**, 174409 (2015).
- [24] J. Romhányi, K. Penc, and R. Ganesh, *Nature Communications* **6**, 6805 (2015).
- [25] A. Mook, J. Henk, and I. Mertig, *Phys. Rev. B* **99**, 014427 (2019).
- [26] A. Mook, J. Henk, and I. Mertig, *Phys. Rev. B* **89**, 134409 (2014).

- [27] A. Mook, J. Henk, and I. Mertig, *Phys. Rev. B* **90**, 024412 (2014).
- [28] S. A. Díaz, J. Klinovaja, and D. Loss, *Phys. Rev. Lett.* **122**, 187203 (2019).
- [29] A. Roldán-Molina, A. S. Nunez, and J. Fernández-Rossier, *New Journal of Physics* **18**, 045015 (2016).
- [30] S. A. Owerre, *Journal of Physics: Condensed Matter* **28**, 386001 (2016).
- [31] P. A. McClarty, X.-Y. Dong, M. Gohlke, J. G. Rau, F. Pollmann, R. Moessner, and K. Penc, *Phys. Rev. B* **98**, 060404 (2018).
- [32] F.-Y. Li, Y.-D. Li, Y. B. Kim, L. Balents, Y. Yu, and G. Chen, *Nature Communications* **7**, 12691 (2016), arXiv:1602.04288 [cond-mat.str-el].
- [33] A. Mook, J. Henk, and I. Mertig, *Phys. Rev. Lett.* **117**, 157204 (2016).
- [34] P. McClarty, F. Krüger, T. Guidi, S. Parker, K. Refson, A. Parker, D. Prabhakaran, and R. Coldea, *Nature Physics* (2017), 10.1038/nphys4117.
- [35] B. Yuan, I. Khait, G.-J. Shu, F. C. Chou, M. B. Stone, J. P. Clancy, A. Paramakanti, and Y.-J. Kim, *Phys. Rev. X* **10**, 011062 (2020).
- [36] M. Elliot, P. A. McClarty, D. Prabhakaran, R. D. Johnson, H. C. Walker, P. Manuel, and R. Coldea, *Nature Communications* **12** (2021), 10.1038/s41467-021-23851-0.
- [37] A. Scheie, P. Laurell, P. A. McClarty, G. E. Granroth, M. B. Stone, R. Moessner, and S. E. Nagler, *Phys. Rev. Lett.* **128**, 097201 (2022).
- [38] A. Scheie, P. Laurell, P. A. McClarty, G. E. Granroth, M. B. Stone, R. Moessner, and S. E. Nagler, *Phys. Rev. B* **105**, 104402 (2022).
- [39] T. Weber, D. M. Fobes, J. Waizner, P. Steffens, G. S. Tucker, M. Böhm, L. Beddrich, C. Franz, H. Gabold, R. Bewley, D. Voneshen, M. Skoulatos, R. Georgii, G. Ehlers, A. Bauer, C. Pfeleiderer, P. Böni, M. Janoschek, and M. Garst, *Science* **375**, 1025 (2022), <https://www.science.org/doi/pdf/10.1126/science.abe4441>.
- [40] Y. Onose, T. Ideue, H. Katsura, Y. Shiomi, N. Nagaosa, and Y. Tokura, *Science* **329**, 297 (2010).
- [41] H. Katsura, N. Nagaosa, and P. A. Lee, *Phys. Rev. Lett.* **104**, 066403 (2010).
- [42] R. Matsumoto and S. Murakami, *Phys. Rev. Lett.* **106**, 197202 (2011).
- [43] R. Matsumoto and S. Murakami, *Physical Review B* **84**, 184406 (2011).
- [44] R. Matsumoto, R. Shindou, and S. Murakami, *Physical Review B* **89**, 054420 (2014).
- [45] S. Murakami and A. Okamoto, *Journal of the Physical Society of Japan* **86**, 011010 (2016).
- [46] Y. Kasahara, K. Sugii, T. Ohnishi, M. Shimozawa, M. Yamashita, N. Kurita, H. Tanaka, J. Nasu, Y. Motome, T. Shibauchi, and et al., *Physical Review Letters* (2018).
- [47] Y. Kasahara, T. Ohnishi, Y. Mizukami, O. Tanaka, S. Ma, K. Sugii, N. Kurita, H. Tanaka, J. Nasu, Y. Motome, and et al., *Nature* **559**, 227–231 (2018).
- [48] R. Hentrich, M. Roslova, A. Isaeva, T. Doert, W. Brenig, B. Büchner, and C. Hess, *Phys. Rev. B* **99**, 085136 (2019).
- [49] S. Shivam, R. Coldea, R. Moessner, and P. McClarty, arXiv e-prints, arXiv:1712.08535 (2017), arXiv:1712.08535 [cond-mat.str-el].
- [50] J. Feldmeier, W. Natori, M. Knap, and J. Knolle, *Phys. Rev. B* **102**, 134423 (2020).
- [51] D. Malz, J. Knolle, and A. Nunnenkamp, *Nature Communications* **10** (2019), 10.1038/s41467-019-11914-2.
- [52] A. Rückriegel, A. Brataas, and R. A. Duine, *Phys. Rev. B* **97**, 081106 (2018).
- [53] A. Mitra, A. Corticelli, P. Ribeiro, and P. A. McClarty, arXiv e-prints, arXiv:2110.02662 (2021), arXiv:2110.02662 [cond-mat.mes-hall].
- [54] See Supplemental Material for further details and additional supporting data.
- [55] J. Zak, *Phys. Rev. B* **23**, 2824 (1981).
- [56] P. A. McClarty and J. G. Rau, *Physical Review B* **100** (2019), 10.1103/physrevb.100.100405.
- [57] W. F. Brinkman and R. J. Elliott, *Proceedings of the Royal Society of London Series A* **294**, 343 (1966).
- [58] W. Brinkman and R. J. Elliott, *Journal of Applied Physics* **37**, 1457 (1966).
- [59] W. Brinkman, *Journal of Applied Physics* **38**, 939 (1967).
- [60] A. Corticelli, R. Moessner, and P. A. McClarty, *Physical Review B* **105** (2022), 10.1103/physrevb.105.064430.
- [61] D. G. Joshi, *Phys. Rev. B* **98**, 060405 (2018).
- [62] M. I. Aroyo, J. M. Perez-Mato, C. Capillas, E. Kroumova, S. Ivantchev, G. Madariaga, A. Kirov, and H. Wondratschek, *Zeitschrift für Kristallographie - Crystalline Materials* **221**, 15 (2006).
- [63] M. I. Aroyo, A. Kirov, C. Capillas, J. M. Perez-Mato, and H. Wondratschek, *Acta Crystallographica Section A* **62**, 115 (2006).
- [64] J. G. Rau, E. K.-H. Lee, and H.-Y. Kee, *Phys. Rev. Lett.* **112**, 077204 (2014).
- [65] H. Kondo and Y. Akagi, *Phys. Rev. Lett.* **127**, 177201 (2021).
- [66] B. Bradlyn, J. Cano, Z. Wang, M. G. Vergniory, C. Felser, R. J. Cava, and B. A. Bernevig, *Science* **353** (2016), 10.1126/science.aaf5037.
- [67] J. Cano, B. Bradlyn, and M. G. Vergniory, *APL Materials* **7**, 101125 (2019).
- [68] A. Bertin, P. Dalmas de Réotier, B. Fåk, C. Marin, A. Yaouanc, A. Forget, D. Sheptyakov, B. Frick, C. Ritter, A. Amato, C. Baines, and P. J. C. King, *Phys. Rev. B* **92**, 144423 (2015).
- [69] V. K. Anand, A. K. Bera, J. Xu, T. Herrmannsdörfer, C. Ritter, and B. Lake, *Phys. Rev. B* **92**, 184418 (2015).
- [70] K. Tomiyasu, K. Matsuhira, K. Iwasa, M. Watahiki, S. Takagi, M. Wakeshima, Y. Hinatsu, M. Yokoyama, K. Ohoyama, and K. Yamada, *Journal of the Physical Society of Japan* **81**, 034709 (2012).
- [71] E. Lhotel, S. Petit, S. Guitteny, O. Florea, M. Ciomaga Hatnean, C. Colin, E. Ressouche, M. R. Lees, and G. Balakrishnan, *Phys. Rev. Lett.* **115**, 197202 (2015).
- [72] J. Xu, V. K. Anand, A. K. Bera, M. Frontzek, D. L. Abernathy, N. Casati, K. Siemensmeyer, and B. Lake, *Phys. Rev. B* **92**, 224430 (2015).
- [73] C. Donnerer, M. C. Rahn, M. M. Sala, J. G. Vale, D. Pincini, J. Strempler, M. Krisch, D. Prabhakaran, A. T. Boothroyd, and D. F. McMorrow, *Phys. Rev. Lett.* **117**, 037201 (2016).
- [74] H. Sagayama, D. Uematsu, T. Arima, K. Sugimoto, J. J. Ishikawa, E. O'Farrell, and S. Nakatsuji, *Phys. Rev. B* **87**, 100403 (2013).
- [75] J. Yamaura, K. Ohgushi, H. Ohsumi, T. Hasegawa, I. Yamauchi, K. Sugimoto, S. Takeshita, A. Tokuda, M. Takata, M. Udagawa, M. Takigawa, H. Harima,

- T. Arima, and Z. Hiroi, *Phys. Rev. Lett.* **108**, 247205 (2012).
- [76] J. N. Reimers, J. E. Greedan, and M. Björgvinsson, *Phys. Rev. B* **45**, 7295 (1992).
- [77] R. Moessner and J. T. Chalker, *Phys. Rev. Lett.* **80**, 2929 (1998), [arXiv:cond-mat/9712063 \[cond-mat.stat-mech\]](#).
- [78] S.-K. Jian and W. Nie, *Phys. Rev. B* **97**, 115162 (2018).
- [79] J. M. Hastings, L. M. Corliss, and C. G. Windsor, *Phys. Rev.* **138**, A176 (1965).
- [80] J. C. Norvell, W. P. Wolf, L. M. Corliss, J. M. Hastings, and R. Nathans, *Phys. Rev.* **186**, 557 (1969).
- [81] I. A. Kibalin, F. Damay, X. Fabrèges, A. Gukassov, and S. Petit, *Phys. Rev. Research* **2**, 033509 (2020).

Supplementary Material for Identifying, and Constructing, Complex Magnon Band Topology

A. Corticelli,¹ R. Moessner,¹ and P. A. McClarty¹

¹*Max Planck Institute for the Physics of Complex Systems,
Nöthnitzer Str. 38, 01187 Dresden, Germany*

arXiv:2203.06678v1 [cond-mat.mes-hall] 13 Mar 2022

Abstract

This section contains supporting information for the paper “Identifying, and constructing, complex magnon band topology”. Section I briefly introduces magnetic space groups and their band representations. EBRs are introduced and their role in accounting for topological bands. Section II discusses band representations in relation to magnons, enumerates all relevant site symmetry groups, reviews linear spin wave theory, the Berry phase for bosons and the implementation of magnetic symmetries within this formalism. Subsection D also describes how to use the Bilbao tables to extract information about EBRs and nodal topology. Section III describes, in detail, several examples of decomposable EBRs for magnons. Finally, Section IV discusses nodal topology originating from EBRs.

I. OVERVIEW OF ELEMENTARY BAND REPRESENTATIONS AND TOPOLOGY

We have described briefly the essential ideas behind the EBR approach to topological band structures. We now make these ideas more precise by first reviewing aspects of the theory of space groups and band representations of these groups.

A. Basic definitions and properties of space groups

A space group G is a group of crystal lattice symmetries. There are 230 such groups in three dimensions that each have a coset decomposition

$$\mathbf{G} = \bigcup_{\alpha} \{R_{\alpha} | \mathbf{t}_{\alpha}\} \mathbf{T} \quad (1)$$

where \mathbf{T} are the primitive lattice translations (forming a normal subgroup) and those of the form $\{g | \mathbf{t}\}$ combining point group element g and non-Bravais translation \mathbf{t} . The combination rules are

$$\{R_1 | \mathbf{t}_1\} \{R_2 | \mathbf{t}_2\} = \{R_1 R_2 | R_1 \mathbf{t}_2 + \mathbf{t}_1\} \quad (2)$$

$$\{R | \mathbf{t}\}^{-1} = \{R^{-1} | -R^{-1} \mathbf{t}\}. \quad (3)$$

A site symmetry group of real space point \mathbf{q} , $G_{\mathbf{q}}$ is the finite subgroup of G that leaves the point invariant. $G_{\mathbf{q}}$ is isomorphic to a point group. A Wyckoff position is the set of

points inside the primitive cell whose site symmetry groups are the same (or, more precisely, in the same conjugacy class). A random point will tend to have only the identity as its site symmetry group and it is then labelled as a general position.

Each point \mathbf{q} has an orbit which is the set of points reached from \mathbf{q} through elements g of the space group. Each Wyckoff position has a multiplicity that counts the number of points in the orbit of the position that live in the same cell.

The above definitions refer to the crystal in real space. But for constructing representations of the space group it is better to move to reciprocal space where the translations are diagonalized. The analogue of a site symmetry group in reciprocal space is the little group which is the set of space group elements that leave momentum \mathbf{k} invariant up to reciprocal lattice vectors. This group contains all translations and it is often useful to mod them out to obtain the so-called little co-group of \mathbf{k} . The analogue of a Wyckoff position in reciprocal space is the star of \mathbf{k} , denoted \mathbf{k}^* which is the set of points in the Brillouin zone reachable by acting with space group elements on \mathbf{k} .

Including magnetic degrees of freedom and time reversal symmetry expands the number of groups from 230 to 1651. The time reversal operator is denoted \mathcal{T} or by apostrophe as $\{E|\mathbf{0}\}'$. Of the 1651 magnetic space groups, there are four types:

1. Type I: the ordinary nonmagnetic space groups G ,
2. Type II: grey groups of the form $G + \mathcal{T}G$ which are relevant to paramagnets,
3. Type III: groups of the form $H + \mathcal{T}(G - H)$ where G and H are non-magnetic,
4. Type IV: black and white groups $G + \mathcal{T}\{E|\mathbf{t}\}H$ composed of time-reversed sublattices.

Magnetically ordered crystals have symmetry groups belonging to classes *I*, *III* and *IV*.

B. Space group band representations

Following Zak, we construct band representations of a space group $\rho_G(g)$ where g is an arbitrary space group element. These are induced from a representation of a subgroup – the site symmetry group for a given position. Physically, we are interested in the case where a lattice is populated with ions carrying some localized orbital degrees of freedom

and tight-binding models derived from these. To induce a representation we need a coset decomposition of the space group

$$G = \bigcup_{\alpha} g_{\alpha} H \quad (4)$$

where H is a subgroup of G – in this case the site symmetry group at \mathbf{q} . The elements g_{α} have the effect of mapping \mathbf{q} to \mathbf{q}_{α} which are all sites in the Wyckoff position of \mathbf{q} .

To see what the band representation looks like, suppose we are given a complete basis of Wannier functions $W_{i\alpha}(\mathbf{r})$ where $i = 1, \dots, d$ runs over onsite degrees of freedom – essentially a set of orbitals, and α runs over different positions in the primitive for a given Wyckoff position (α therefore runs over 1 to n , the multiplicity of that position). Translations map the Wannier functions to different primitive cells (\mathcal{N} in number) giving $d \times n \times \mathcal{N}$ distinct Wannier functions.

Going to momentum space

$$v_{i\alpha}(\mathbf{k}, \mathbf{r}) = \sum_{\mathbf{t}} e^{i\mathbf{k}\cdot\mathbf{t}} W_{i\alpha}(\mathbf{r} - \mathbf{t}) \quad (5)$$

provides a basis of states on which the band representation can act.

$$[\rho_G(g)] v_{i\alpha}(\mathbf{k}, \mathbf{r}) = e^{-i(R\mathbf{k})\cdot\mathbf{t}_{\beta\alpha}} \sum_{j=1}^d [\rho(h)]_{ji} v_{j\beta}(R\mathbf{k}, \mathbf{r}). \quad (6)$$

In this expression space group element g and site symmetry group element h are related by

$$g = g_{\alpha}^{-1} \{E | \mathbf{t}_{\beta\alpha}\} g_{\beta} h \quad (7)$$

where $\mathbf{t}_{\beta\alpha} = g\mathbf{q}_{\alpha} - \mathbf{q}_{\beta}$ and R is the point group element in g . So the α and β coset representatives are fixed given g and h .

Evidently the band representation links \mathbf{k} and $R\mathbf{k}$. In the case where $R\mathbf{k}$ is the same as \mathbf{k} up to a reciprocal lattice vector, the corresponding block in the band representation is a representation of the little group at \mathbf{k} . However, the band representation has off-diagonal blocks that contain information about how different points in the zone are connected.

C. Elementary Band Representations

A band representation constructed via the method detailed in the previous section may be decomposable into the direct sum of two or more band representations. If this is the case it is called *composite* and otherwise *elementary*. More precisely, we first define an equivalence

between two band representations $\rho_G^{(1)}(h, \mathbf{k})$, $\rho_G^{(2)}$ if it is possible to find unitary $S(\lambda; h, \mathbf{k})$ such that $\lambda : [0, 1]$ tunes smoothly from one of the two band representations to the other: $S(0; h, \mathbf{k}) = \rho_G^{(1)}(h, \mathbf{k})$ and $S(1; h, \mathbf{k}) = \rho_G^{(2)}(h, \mathbf{k})$. Such a function preserves the quantization of any Wilson loops in momentum space. This notion of equivalence is explicitly realized by inducing a BR from two distinct sites \mathbf{q}_1 , \mathbf{q}_2 with respective site symmetry groups $G_{\mathbf{q}_1}$ and $G_{\mathbf{q}_2}$. A line between the two points is associated with SSG $G_{\mathbf{q}_1} \cap G_{\mathbf{q}_2}$ and by moving along this line the induced band representation defines $S(\lambda; h, \mathbf{k})$. It follows that equivalence of band representations amounts to being able to find a site that interpolates between the SSGs of the endpoint BRs. With this notion of equivalence, we now define composite BRs to be those that are equivalent to direct sums of BRs. An EBR can be characterized by the multiplicity of irreps at all high symmetry momenta.

Elementary band representations (EBRs), thus defined, are the fundamental symmetry-derived bands built from localized orbitals. In contrast, as we noted in the main text, the key distinguishing feature of topological bands is that they are not Wannier localizable.

The foundation of TQC is a complete enumeration of the EBRs for all 1651 magnetic space groups together with the compatibility relations that constrain how little groups at particular momenta are connected. This task, while considerable, is possible at all because the number of EBRs is finite, bounded by the number of irreps of SSGs at all Wyckoff positions of all magnetic space groups. In addition, many BRs induced in this way are actually composite. It turns out that to capture all EBRs it suffices (modulo some carefully characterized exceptions) to consider only the irreps of so-called *maximal* SSGs. Maximal SSGs are defined as SSGs $G_{\mathbf{q}}$ such that there is no finite group H for space group G for which $G_{\mathbf{q}} \subset H \subset G$. Given each EBR, one may further ask whether it is decomposable or not by computing the compatibility relations for the constituent bands.

The result is that there are 20206 magnetic EBRs belonging to the 1651 (single-valued or spinless) magnetic space groups of which 1907 are decomposable. For our purposes, these are the relevant magnetic space groups. A similar enumeration has been carried out also for the doubled (or spinful) magnetic space groups. A complete tabulation of these EBRs organized by magnetic space group may be found on the Bilbao Crystallographic Server [1, 2].

Given a set of bands that are energetically isolated, one may then assess whether they can be decomposed, on their own, into a combination of EBRs (with non-negative integer

coefficients). If so, the bands are topological trivial (or fragile). If not they are topologically non-trivial. In this situation, should the coefficients be integer-valued including negative integers the topology is fragile and otherwise it is stable.

In addition, single EBRs may be composed of multiple bands that are not forced to be connected by compatibility relations. In the main text we assign particular importance to such cases. These *decomposable* EBRs have the property that at least one of the disconnected component set of bands must be topological. In cases where one component is trivial the decomposable EBR is a self-contained case of fragile topology. In the examples we have explored, the two disconnected components are both topological.

EBR are also useful for assessing the existence of topological semimetals. These arise from connected EBRs where, in electronic systems, the bands are filled up to touching points or lines within the EBR.

All these insights have been put to use diagnosing band topology in the electronic band structures of materials. Given the symmetry group of a crystalline material and the Wyckoff positions and orbitals of the constituent ions, symmetry places strong constraints on the EBRs that may occur in the band structure. From the computed band structure (usually performed along high symmetry directions in momentum space), one may compute the multiplicities of the irreps at these momenta. From the identities of the tabulated EBRs one may then make the assessment of whether some given set of bands is reducible into EBRs.

This approach massively generalizes the Fu-Kane criterion for two-dimensional topological insulators that, in the original formulation, allows one to compute the Chern number purely from discrete data at high symmetry momenta. By now, analogous formulas called symmetry indicator formulas are known for all space groups and all (double-valued) magnetic space groups each of which allows one to diagnose directly from irrep multiplicities whether the band or group of bands is trivial or not.

II. MAGNETIC SYMMETRY AND MAGNONS

In this section, we briefly review the essential facts about magnons and their symmetries. Magnons are to be understood as coherent magnetic excitations about some spontaneous or field-induced magnetic structure. We focus our attention on commensurate magnetic order characterized by some periodic arrangement of moments with nonzero vacuum expectation

value $\langle J_i^\alpha \rangle$ for sites i and components α .

To understand magnon symmetries it is helpful to begin with the magnetic Hamiltonian describing coupled magnetic moments on a lattice. The lattice itself has symmetries specified by one of the 230 space groups. The Hamiltonian may have higher symmetry however: spin rotation symmetry for Heisenberg couplings or time reversal symmetry when the couplings are of even degree in the moments. In the most general case, the magnetic Hamiltonian has a spin-space symmetry composed of elements with somewhat decoupled spin rotation symmetries. However, in this paper, we restrict our attention to the case of strong spin-orbit coupled moments so that the moments are locked to spatial transformations. Under this assumption, the magnetic space groups are adequate to describe all the relevant symmetries. An important implication of this assumption is that we are explicitly or implicitly considering the case where the magnetic interactions of all types allowed by spin-space-locked symmetry are present and significant. In other words, the exchange is considered to be maximally anisotropic.

From the point of view of materials, the restriction to magnetic space groups is strictly speaking correct as spin-orbit coupling is always present even when the orbital moment is quenched at the single ion level. Anisotropies in the exchange will be present even in such instances. However, for practical purposes, this assumption is too severe as there are many materials where the interactions are experimentally indistinguishable from the Heisenberg limit or where the spin-orbit is weak enough that a residual spin-space symmetry remains. Such cases are discussed in greater detail in Ref. 3.

For such cases, we stress that the techniques we employ can be used straightforwardly to study spin-space groups also. But since they have not yet been tabulated we leave a systematic study of their topological properties as a task for the future.

As discussed above, magnetic space groups can be classified into four different types. The magnetic space group symmetries of the magnetic Hamiltonian fall into classes I or II. Respectively these are the ordinary space groups (I) and groups of the form $G + \mathcal{T}G$ where \mathcal{T} is the time reversal operation (II).

The interplay between spatial and time reversal symmetries can become more elaborate in the presence of magnetic order. Magnetic order breaks the symmetry group of the Hamiltonian G_H down to G_M which is the set of symmetry elements – combinations of point group elements (e.g. rotations, mirrors), translations and time reversal – that leave the

magnetic structure, $\langle J_i^z \rangle$, invariant where the z component refers to a local frame aligned with the ordered moment. Since the magnetic order breaks physical time reversal symmetry spontaneously if it is not explicitly broken at the Hamiltonian level, G_M cannot be a type II magnetic space group. This leaves the 1421 type I, III and IV magnetic space groups as possible magnon symmetry groups.

To build a band representation we require the magnetic site symmetry groups. These can be viewed as the set of elements of G_M that both leave the site invariant up to a primitive translation and leave the magnetic order invariant. Thus, given \mathbf{q}_1 an orbit of the Wyckoff position, applying the elements of magnetic site symmetry group $G_{\mathbf{q}_1}$ the condition that the magnetic order by left invariant is:

$$g_\alpha J_{\mathbf{q}_1}^z = J_{\mathbf{q}_1}^z \quad \forall g_\alpha \in G_{\mathbf{q}_1}. \quad (8)$$

Expressed another way, J^z must transform like the total symmetric irrep of $G_{\mathbf{q}_1}$. Those Wyckoff positions that do not satisfy this constraint are not compatible with order and must reduce to Wyckoff positions of a less symmetric magnetic space group. Using this constraint we recover the magnetic structures compatible with the magnetic space group by listing the Wyckoff positions compatible with order and applying:

$$g_i J_{\mathbf{q}_1}^z : R_i^{z\alpha} J_{\mathbf{q}_i}^\alpha \quad \forall g_i : G = \bigcup_i g_i (G_{\mathbf{q}_i} \times T) \quad (9)$$

where \mathbf{q}_i is the orbit of the Wyckoff position relative to g_i and $R_i^{z\alpha}$ is the rotation matrix associated to g_i .

The site symmetry group of the magnetic ions must be isomorphic to one of the 122 magnetic point groups. These are divided into the 32 crystallographic point groups, the 32 grey point groups with pure time-reversal operators and 58 black and white point groups with mixed time-reversal elements. The constraint that the J_z component transform as the totally symmetric representation of the site symmetry group restricts the possibilities to a subset of the magnetic point groups. Of the 32 crystallographic point groups, 13 preserve the moment, of the 58 black and white point groups there are 18 moment preserving groups. None of the grey groups are possible since time-reversal does not preserve the magnetic order. In total, 31 out of the 122 magnetic point groups are possible magnetic site symmetry groups. These are listed in Table I.

We are now in a position to discuss magnons. These are transverse modes built from the J_i^\pm components. In order to build up band representations for magnons, the starting

Magnetic Site Symmetry Group	(J^+, J^-) irreps
1, 2', m'	2A
-1, 2'/m'	2A _g
2, 2'2'2, m'm'2	2B
m, m'm2'	2A''
2/m, m'm'm	2B _g
4, 42'2', 4m'm'	¹ E + ² E
-4, -42'm'	¹ E + ² E
4/m, 4/mmm'm'	¹ E _g + ² E _g
3, 32', 3m'	¹ E + ² E
-3, -3m'	¹ E _g + ² E _g
6, 62'2', 6m'm'	¹ E ₂ + ² E ₂
-6, -6m'2'	¹ E'' + ² E''
6/m, 6/mmm'm'	¹ E _{2g} + ² E _{2g}

TABLE I. The 31 site symmetry groups compatible with magnetic ordered systems. The groups with same unitary subgroup are list in the same line and the relative unitary irreps of the transverse spin components for spin wave are listed in the right column. The notation of the irreps follows Ref. [4].

point is the set of site symmetry groups for which J_z transforms as the totally symmetric representation listed in Table I. Given these groups, we may establish how the transverse spin components transform and this information completely fixes the allowed representations of the SSG for the purposes of building the band representation. These SSG representations are also given in Table I.

From the table we see that J_i^\pm will, in general, induce a pair of EBRs, which are the same if real or complex conjugates of one other if complex. This fact reflects distinctive paraunitarity of the bosonic Bogoliubov diagonalization that produces two set of bands at positive and negative energies with complex conjugated eigenvector thus redundantly encoding information about the band structure. It is important to note that the Herring criterion forbids these complex conjugated EBRs from pairing within a single EBR when the anti-unitary elements are considered. This is a result of the magnetic order constraint

preserving J^z , which translate in the prohibition to mix of J^+ and J^- .

What distinguishes band representations induced from these SSG representations? We have seen that the interesting band representations are the EBRs obtained from the maximal Wyckoff positions since all the other BRs can be seen as composite of these. Therefore the EBRs can be divided into two groups for magnons. One group is induced from maximal Wyckoff positions compatible with magnetic order – they can be induced directly starting from the orbitals $J_{\mathbf{q}}^{\pm}$ on the maximal Wyckoff positions \mathbf{q} themselves. The second group has maximal Wyckoff positions that are not compatible with magnetic order or comes from representations describing different orbitals than $J_{\mathbf{q}}^{\pm}$. These can only be induced as a part of a composite representation from orbitals $J_{\mathbf{q}_L}^{\pm}$ from a less symmetric Wyckoff position \mathbf{q}_L . In practice, the first group allows one to construct magnon spectra composed of a single EBR, with straightforward topological identification once a gap is present. All the *decomposable* EBRs which can appear among this kind of single EBRs in magnon band structures are listed in Tab. X.

A. Linear Spin Wave Theory

So far we have discussed the transformation properties of magnons at a relatively abstract level. To connect to the magnon band structures of materials we use the standard Holstein-Primakoff identity

$$\hat{J}^z = S - \hat{a}^\dagger \hat{a} \tag{10}$$

$$\hat{J}^+ = \sqrt{2S} \sqrt{1 - \frac{\hat{a}^\dagger \hat{a}}{2S}} \hat{a} = \sqrt{2S} \left(1 - \frac{\hat{a}^\dagger \hat{a}}{4S} \right) \hat{a} + \dots \tag{11}$$

$$\hat{J}^- = \sqrt{2S} \hat{a}^\dagger \sqrt{1 - \frac{\hat{a}^\dagger \hat{a}}{2S}} = \sqrt{2S} \hat{a}^\dagger \left(1 - \frac{\hat{a}^\dagger \hat{a}}{4S} \right) + \dots \tag{12}$$

where the spins are of length S and the bosons a , a^\dagger satisfy the usual commutation relations $[\hat{a}, \hat{a}^\dagger] = 1$. Linearizing these gives

$$\hat{J}_{\mathbf{ka}}^+ \rightarrow \sqrt{2S} \hat{a}_{\mathbf{ka}} \tag{13}$$

$$\hat{J}_{\mathbf{ka}}^- \rightarrow \sqrt{2S} \hat{a}_{-\mathbf{ka}}^\dagger. \tag{14}$$

Using this bosonic representation for the spins and expanding the magnetic Hamiltonian around the mean field ground state leads to the quadratic Hamiltonian

$$H_{\text{SW}} = \frac{S}{2} \sum_{\mathbf{k}} \hat{\mathbf{Y}}^\dagger(\mathbf{k}) \begin{pmatrix} \mathbf{A}(\mathbf{k}) & \mathbf{B}(\mathbf{k}) \\ \mathbf{B}^*(-\mathbf{k}) & \mathbf{A}^*(-\mathbf{k}) \end{pmatrix} \hat{\mathbf{Y}}(\mathbf{k}) \equiv \frac{S}{2} \sum_{\mathbf{k}} \hat{\mathbf{Y}}^\dagger(\mathbf{k}) \mathbf{M}(\mathbf{k}) \hat{\mathbf{Y}}(\mathbf{k}) \quad (15)$$

where

$$\hat{\mathbf{Y}}^\dagger(\mathbf{k}) = \left(\hat{a}_{\mathbf{k}1}^\dagger \dots \hat{a}_{\mathbf{k}m}^\dagger \hat{a}_{-\mathbf{k}1} \dots \hat{a}_{-\mathbf{k}m} \right) \quad (16)$$

and the $\mathbf{A}_{ab}(\mathbf{k})$ and $\mathbf{B}_{ab}(\mathbf{k})$ depend on the exchange couplings in the local quantization frame as follows:

$$\mathbf{A}_{ab}(\mathbf{k}) = \tilde{\mathbf{J}}_{ab}^{+-}(\mathbf{k}) - \delta_{ab} \sum_c \tilde{\mathbf{J}}_{ac}^{zz}(\mathbf{0}) \quad (17)$$

$$\begin{aligned} \mathbf{B}_{ab}(\mathbf{k}) &= \frac{1}{2} \left(\tilde{\mathbf{J}}_{ab}^{xx}(\mathbf{k}) - \tilde{\mathbf{J}}_{ab}^{yy}(\mathbf{k}) - i\tilde{\mathbf{J}}_{ab}^{xy}(\mathbf{k}) - i\tilde{\mathbf{J}}_{ab}^{yx}(\mathbf{k}) \right) \\ &= \tilde{\mathbf{J}}_{ab}^{--}(\mathbf{k}). \end{aligned} \quad (18)$$

Note that these expressions with the factor one-half define $\tilde{\mathbf{J}}_{ab}^{\alpha\beta}$ for $\alpha, \beta = \pm$.

The diagonalizing transformation

$$\mathbf{V}^\dagger(\mathbf{k}) \mathbf{M}(\mathbf{k}) \mathbf{V}(\mathbf{k}) = \mathbf{\Lambda}(\mathbf{k}) \quad (19)$$

on Eq. 15 to find the spin wave spectrum must preserve the commutation relations

$$[\Upsilon_a, \Upsilon_b^\dagger] = \eta_{ab} \quad (20)$$

where $\eta_{ab} = 1$ if $a = b \leq m$ and $\eta_{ab} = -1$ if $a = b \geq m + 1$ and zero otherwise. Here

$$\mathbf{\Lambda}(\mathbf{k}) = \begin{pmatrix} \epsilon_1(\mathbf{k}) & \epsilon_2(\mathbf{k}) & \dots & \epsilon_1(-\mathbf{k}) & \epsilon_2(-\mathbf{k}) & \dots \end{pmatrix} \quad (21)$$

In order for both conditions to be satisfied \mathbf{V} is not unitary in general, as would be the case for fermions, but *paraunitary* meaning that

$$\mathbf{V}(\mathbf{k}) \boldsymbol{\eta} \mathbf{V}^\dagger(\mathbf{k}) = \boldsymbol{\eta}.$$

The transformation is unitary only in the case where the number non-conserving terms in the Hamiltonian vanish.

B. Berry Phase and Berry Curvature

The Berry phase is of central importance to band topology. For bosonic systems the Berry phase for band n is

$$A_\mu^{(n)}(\mathbf{k}) = i \text{Tr} \left[\boldsymbol{\Gamma}^{(n)} \boldsymbol{\eta} \mathbf{V}^\dagger(\mathbf{k}) \boldsymbol{\eta} \partial_{k_\mu} \mathbf{V}(\mathbf{k}) \right]. \quad (22)$$

where

$$\mathbf{P}_\mu = \mathbf{V}(\mathbf{k})\Gamma^{(n)}\boldsymbol{\eta}\mathbf{V}^\dagger(\mathbf{k})\boldsymbol{\eta} \quad (23)$$

is the projector onto the n th band.

From this one may compute the Berry curvature for the n th band

$$F_\mu^{(n)}(\mathbf{k}) = \epsilon_{\mu\rho\sigma}\partial_{k_\rho}A_\sigma^{(n)}(\mathbf{k}). \quad (24)$$

The integral of this curvature over a 2D slice through the Brillouin zone is quantized and deformable only by closing a band gap.

$$C^{(n)} = \frac{1}{2\pi} \int_{2DBZ} d^2\mathbf{k} F^{(n)}(\mathbf{k}) \quad (25)$$

C. Symmetries

In this section, we show how to build a representation of the group elements for magnons. The relevant group is composed of those elements of the full magnetic Hamiltonian that leave the magnetic structure invariant, \mathbf{G}_M . The spin wave Hamiltonian is expressed in the basis of transverse spin components and is invariant under this group. Thus in the local quantization frame,

$$\hat{J}_{\mathbf{k}a}^+ \rightarrow \sqrt{2S}\hat{a}_{\mathbf{k}a} \quad (26)$$

$$\hat{J}_{\mathbf{k}a}^- \rightarrow \sqrt{2S}\hat{a}_{-\mathbf{k}a}^\dagger. \quad (27)$$

Leaving time reversal aside for now, a group element takes the form $S = \{g | \mathbf{t}\}$ acting on a lattice site $\mathbf{R}_i + \mathbf{r}_a$ as

$$\mathbf{R}_i + \mathbf{r}_a \rightarrow g(\mathbf{R}_i + \mathbf{r}_a) + \mathbf{t} = \mathbf{R}_j + \mathbf{r}_b. \quad (28)$$

Under this transformation, local moments are mapped from one lattice position to another preserving the moment orientation and, in general, rotating the transverse components.

Under a C_n rotation of the transverse components about the moment orientation

$$C_n \hat{J}_{ia}^\pm C_n^{-1} = e^{-2\pi i/n} \hat{J}_{ia}^\pm. \quad (29)$$

and we further note that inversion leaves moments invariant as they are pseudo-vectors and that reflections are equivalent to an inversion times a C_2 with axis perpendicular to the mirror plane.

The space group element S acting on \hat{J}_{ia}^\pm gives

$$U_S \hat{J}_{ia}^\pm U_S^{-1} = [U_g^\pm]_{ab} \hat{J}_{jb}^\pm \quad (30)$$

where $[U_g^\pm]_{ab}$ permutes sublattices and carries out local rotations. We then Fourier transform as

$$J_{ia}^\alpha = \frac{1}{\sqrt{N}} \sum_{\mathbf{k}} J_{\mathbf{k}a}^\alpha e^{i\mathbf{k} \cdot (\mathbf{R}_i + \nu \mathbf{r}_a)} \quad (31)$$

where $\nu = 0, 1$ keeps track of both standard conventions. A short calculation reveals that

$$U_S \hat{J}_{\mathbf{k}a}^\pm U_S^{-1} = [U_g^\pm]_{ab} \hat{J}_{g\mathbf{k}b}^\pm \exp[-i(g\mathbf{k}) \cdot ((1-\nu)(\mathbf{r}_b - g\mathbf{r}_a) - \mathbf{t})]. \quad (32)$$

On the basis of this transformation law and the invariance of H_{SW} , one may show that

$$M_{ab}(\mathbf{k}) = [U_g^\pm]_{am}^\dagger M_{mn}(g^{-1}\mathbf{k}) [U_g^\pm]_{nb}. \quad (33)$$

Including time reversal symmetries as follows

$$\hat{\mathcal{T}}_i \hat{\mathcal{T}}^{-1} = -i \quad (34)$$

$$\hat{\mathcal{T}} \hat{J}_{ia}^\pm \hat{\mathcal{T}}^{-1} = -\hat{J}_{ia}^\mp \quad (35)$$

$$\hat{\mathcal{T}} \hat{J}_{\mathbf{k}a}^\pm \hat{\mathcal{T}}^{-1} = -\hat{J}_{-\mathbf{k}a}^\mp \quad (36)$$

completes the set of transformations on transverse components of the magnetic moment allowing one to construct a representation on the basis of $a_{\mathbf{k}a}$ and $a_{-\mathbf{k}a}^\dagger$.

D. Use of Bilbao Crystallographic Server MBANDREP tool for magnons

Here we explain briefly how to make practical use of the magnetic band representation tool MBANDREP on the Bilbao Crystallographic Server for magnon systems [5, 6]. This tool is very useful for topological magnons for two main purposes: identifying decomposable (topological gapped) EBRs and finding compatibility relations constraining possible topological nodal features. Once interesting cases have been established on symmetry grounds one may use the symmetry data to build models with nontrivial magnon band topology as we show.

Given a magnetic space group in the BNS convention, this tool shows which band representations can be induced from a particular Wyckoff position. Each Wyckoff position may induce either an elementary or a composite band representation.

Wyckoff pos.		2c(32',3)	2c(32',3)	2c(32',3)	2c(32',3)	2c(32',3)	2c(32',3)
Band-rep.		${}^1E \uparrow G(2)$	${}^2E \uparrow G(2)$	$A_1 \uparrow G(2)$	${}^1E \uparrow G(2)$	${}^2E \uparrow G(2)$	$\bar{E} \uparrow G(2)$
Decomposable Indecomposable		Decomposable	Decomposable	Decomposable	Decomposable	Decomposable	Decomposable
$\Gamma:(0,0,0)$	$\Gamma:(0,0,0)$	$\Gamma_3^+(1) \oplus \Gamma_3^-(1)$	$\Gamma_2^+(1) \oplus \Gamma_2^-(1)$	$\Gamma_1^+(1) \oplus \Gamma_1^-(1)$	$\bar{\Gamma}_5(1) \oplus \bar{\Gamma}_8(1)$	$\bar{\Gamma}_6(1) \oplus \bar{\Gamma}_9(1)$	$\bar{\Gamma}_4(1) \oplus \bar{\Gamma}_7(1)$
$A:(0,0,1/2)$	$A:(0,0,1/2)$	$A_3^+(1) \oplus A_3^-(1)$	$A_2^+(1) \oplus A_2^-(1)$	$A_1^+(1) \oplus A_1^-(1)$	$\bar{A}_5(1) \oplus \bar{A}_8(1)$	$\bar{A}_6(1) \oplus \bar{A}_9(1)$	$\bar{A}_4(1) \oplus \bar{A}_7(1)$
$H:(1/3,1/3,1/2)$	$H:(1/3,1/3,1/2)$	$H_1(1) \oplus H_2(1)$	$H_1(1) \oplus H_3(1)$	$H_2(1) \oplus H_3(1)$	$\bar{H}_4(1) \oplus \bar{H}_6(1)$	$\bar{H}_4(1) \oplus \bar{H}_5(1)$	$\bar{H}_5(1) \oplus \bar{H}_6(1)$
$K:(1/3,1/3,0)$	$K:(1/3,1/3,0)$	$K_1(1) \oplus K_2(1)$	$K_1(1) \oplus K_3(1)$	$K_2(1) \oplus K_3(1)$	$\bar{K}_4(1) \oplus \bar{K}_6(1)$	$\bar{K}_4(1) \oplus \bar{K}_5(1)$	$\bar{K}_5(1) \oplus \bar{K}_6(1)$
$L:(1/2,0,1/2)$	$L:(1/2,0,1/2)$	$L_1^+(1) \oplus L_1^-(1)$	$L_1^+(1) \oplus L_1^-(1)$	$L_1^+(1) \oplus L_1^-(1)$	$\bar{L}_2(1) \oplus \bar{L}_3(1)$	$\bar{L}_2(1) \oplus \bar{L}_3(1)$	$\bar{L}_2(1) \oplus \bar{L}_3(1)$
$M:(1/2,0,0)$	$M:(1/2,0,0)$	$M_1^+(1) \oplus M_1^-(1)$	$M_1^+(1) \oplus M_1^-(1)$	$M_1^+(1) \oplus M_1^-(1)$	$\bar{M}_2(1) \oplus \bar{M}_3(1)$	$\bar{M}_2(1) \oplus \bar{M}_3(1)$	$\bar{M}_2(1) \oplus \bar{M}_3(1)$

FIG. 1. Screenshot from MBANDREP tool on Bilbao Crystallographic Server for the magnetic space group $P\bar{3}1m'$ (#162.77) and maximal Wyckoff position $2c$. In the red circle the relevant band representations for magnons. The use of the table is discussed in the main text.

As an example, suppose we want to know if a topological gap is possible for the honeycomb Heisenberg-Kitaev FM [111] without an explicit calculation (see also Sec. III A). The essential ingredients to make this determination are the symmetries of the underlying crystal lattice, which are conserved by the exchange coupling, and the magnetic order. In this case, the honeycomb lattice can be seen as a 3D space group $P6/mmm$, with associated point group D_{6h} ($6/mmm$), and Wyckoff position $2c$. The Kitaev coupling does not preserve the C_6 rotation, breaking the point group down to D_{3d} ($-3m$). In addition, the FM [111] ordering out of plane breaks the two-fold rotations in the plane and relative mirrors, which can only be restored in combination with time-reversal symmetry thus forming the magnetic point group $-3m'$. Therefore, the relevant magnetic space group is $P\bar{3}1m'$ (#162.77). In listing the symmetries of the exchange Hamiltonian we should also consider possible spin-rotation symmetries. For the case of the Heisenberg-Kitaev model there are extra spin rotations symmetries that form a D_2 group but these are killed off by the [111] magnetic order as discussed in Ref. 3. Having established the magnetic space group and the Wyckoff position, we can use the MBANDREP tool and analyze the relevant band representations.

Wyckoff pos.		$16c(\bar{3}m',\bar{3})$
Band-rep.		${}^1E_g \uparrow G(4)$
Decomposable Indecomposable		Indecomposable
$\Gamma:(0,0,0)$	$\Gamma:(0,0,0)$	$\Gamma_3^+(1) \oplus \Gamma_4^+(3)$
$L:(1/2,1/2,1/2)$	$L:(1/2,1/2,1/2)$	$L_1^-(1) \oplus L_2^-(1) \oplus L_3^+(1) \oplus L_3^-(1)$
$W:(1/2,1,0)$	$W:(1/2,1,0)$	$2 W_1(2)$
$X:(0,1,0)$	$X:(0,1,0)$	$X_1(2) \oplus X_2(2)$
$\Delta:(0,v,0)$	$\Delta:(0,v,0)$	$\Delta_1(1) \oplus \Delta_2(1) \oplus \Delta_3\Delta_4(2)$
$\Lambda:(u,u,u)$	$\Lambda:(u,u,u)$	$\Lambda_1(1) \oplus \Lambda_2(1) \oplus 2 \Lambda_3(1)$
$Q:(1/2,v,1-v)$	$Q:(1/2,v,1-v)$	$4 Q_1(1)$
$\Sigma:(u,u,0)$	$\Sigma:(u,u,0)$	$2 \Sigma_1(1) \oplus 2 \Sigma_2(1)$
$V:(u,1,0)$	$V:(u,1,0)$	$2 V_1(2)$
$A:(u,v,0)$	$A:(u,v,0)$	$2 A_1(1) \oplus 2 A_2(1)$
$C:(u,u,w)$	$C:(u,u,w)$	$4 C_1(1)$
$GP:(u,v,w)$	$GP:(u,v,w)$	$4 GP_1(1)$

FIG. 2. Screenshot from MBANDREP tool on Bilbao Crystallographic Server for the magnetic space group 227.131 Wyckoff position 16c and EBR induced from 1E_g . In the red circles the representations showing the 3-fold nodal point at Γ and the two 2-fold nodal lines at Δ and V .

In Fig. 1 we give an example of a MBANDREP table. In the first row the Wyckoff position (2c) is indicated together with its magnetic site-symmetry group and unitary subgroup ($32', 3$). In the second row, the different band representations from unitary irreps of the site-symmetry group are shown. In the third row, the band representation is labelled as either decomposable (possible topological gap) or indecomposable (no gap possible) as determined from the compatibility relations. In case it is decomposable, the tool further shows all the possible split branches. Finally, the subsequent rows show the band representation subduced to irreps of the maximal high symmetry points in reciprocal space.

Of the six possible band representations here we can immediately neglect the double valued ones (last 3 columns with barred irreps) and focus on the single valued ones as

is appropriate for spin waves. In particular, the orbitals $J_{\mathbf{q}}^{\pm}$ transform under the unitary subgroup of the site-symmetry group 3 as irreps ${}^1E, {}^2E$ as we can see in Tab. I. Therefore we are interested in the EBR in the red circle ${}^1E \uparrow G(2)$ and ${}^2E \uparrow G(2)$, where the number in parentheses indicates the number of bands given by this Wyckoff position (here Wyckoff $2c$ is a two sublattices basis producing two bands). One of the irreps 1E or 2E is associated to the positive energies bands while the complex conjugated one to the negative bands produced by Bogoliubov diagonalization. We therefore see immediately that the orbital $J_{\mathbf{q}}^{\pm}$ induces a decomposable EBR, meaning that a gap is topological. A list of all possible single decomposable EBRs for magnons can be found in Tab. X. This table can be used to straightforwardly identify a topological gap, without accessing the full server details or computing explicitly the representations of the band structure. Indeed if the magnetic material one is looking at (or the model intended to be constructed) is present in the table, non-trivial magnon topology is guaranteed once a gap is present.

One may, with this information, build a model exhibiting this topological gap. To do this, it is necessary to enforce the symmetries of the lattice at the level of the magnetic Hamiltonian taking care not to allow spin-space symmetries. Physically this means that the model should be spin-orbit coupled and include, in principle, all symmetry-allowed exchange couplings. The Kitaev-Heisenberg model includes only a subset of the allowed couplings to nearest neighbor but (i) the magnetic order is sufficient to break down the residual symmetries and (ii) including further couplings such as Γ, Γ' [7] preserves the band topology.

Finally we detail how to identify topological nodal models using the magnetic band representation. As an example we take the magnetic group 227.131 Wyckoff position $16c$ relevant for pyrochlore AIAO order discussed in Sec. IV A. From the Bilbao server, we extract the information in Fig. 2. Here we are interested in the EBR ${}^1E_g \uparrow G(4)$ having 4 bands (or alternatively the conjugated one, showing the same enforced degeneracies). To identify possible symmetry enforced degeneracies we need to inspect the subduced irreps at the high symmetry points/lines/surface in the first Brillouin zone. At the Γ point the EBR will be composed of two irreps, $\Gamma_3^1(1) + \Gamma_4^+(3)$, where the number in parentheses is the dimension of the irrep, indicating the presence of a 3-fold degenerate nodal point. In addition we can identify one 2-fold nodal line at $\Delta = (0, v, 0) = [\Gamma - X]$ and 2 others at $V = (u, 1, 0) = [X - W]$, marked with red circles (the coordinate are given in reciprocal

lattice basis). These symmetry enforced degeneracies can then be checked by carrying out a direct LSW calculation, as in Fig. IV.

III. DECOMPOSABLE EBR FOR MAGNONS: EXAMPLES

A. Honeycomb Heisenberg-Kitaev FM [111] model

For simplicity the first case considered is the two dimensional Honeycomb Heisenberg-Kitaev ferromagnet. It has already been shown in Ref. [7, 8] that the model hosts a gap with a non-trivial Chern invariant for the out of plane polarization, [111] direction in Kitaev spin coordinate system. In fact the gap closes only for polarizations along $[xy0]$, $[x0z]$, $[0yz]$ (where an emergent spin-space symmetry enforces the gap closure [3]). In this section, we focus on the case where the moment is along [111] and show that the nontrivial topology can be understood from the perspective of a decomposable EBR.

1. Crystal structure

The crystal structure we consider is an honeycomb lattice with an edge-shared octahedral environment around the sites so that Kitaev couplings are allowed by symmetry. The magnetic moments are polarized perpendicular to the honeycomb plane. This magnetic structure is described by the magnetic group $F\bar{3}1m'$ (#162.77 in BNS setting) with Wyckoff position $2c$ that has site symmetry group $32'$. The lattice primitive vectors are:

$$\mathbf{a}_1 = (\sqrt{3}/2, 3/2), \quad \mathbf{a}_2 = (\sqrt{3}/2, -3/2) \quad (37)$$

and basis coming from Wyckoff position $2c$ is (origin at the center of the hexagon):

$$\boldsymbol{\delta}_1 = (\sqrt{3}/2, -1/2), \quad \boldsymbol{\delta}_2 = (\sqrt{3}/2, 1/2). \quad (38)$$

Taking into account the octahedral environment the relevant point group under which the exchange is left invariant is D_{3d} with nontrivial symmetries including three-fold rotations about the hexagonal centers, three two-fold rotational symmetries about axes through opposite hexagonal vertices and inversion symmetry again about the hexagonal centers. Once the out of plane [111] magnetization is taken into consideration, the two-fold rotations are symmetries only in combination with time-reversal to restore the spin direction. The generators

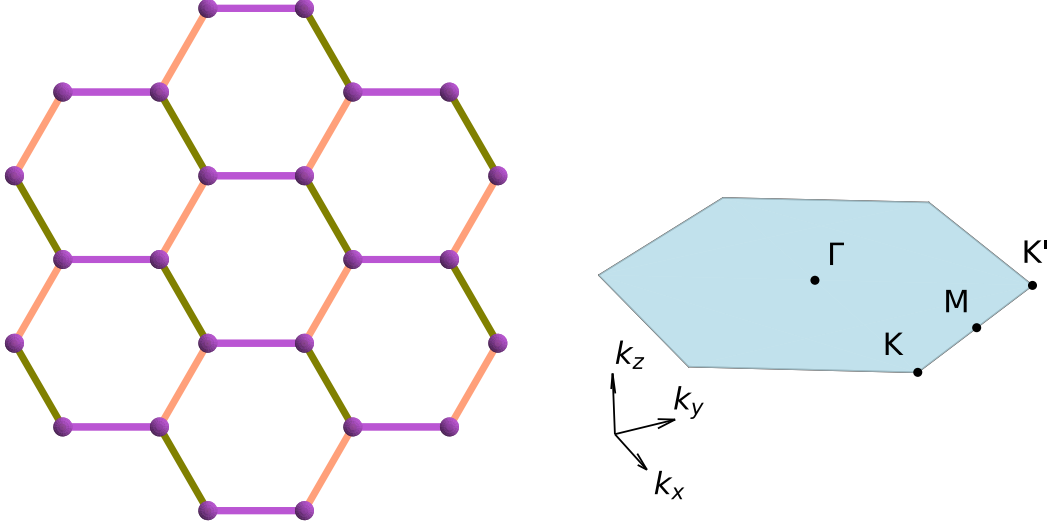


FIG. 3. The honeycomb lattice and its first Brillouin zone. In the lattice the bond colors (purple, orange, green) indicate the x , y , z pattern of the Kitaev couplings. In the Brillouin zone the high symmetry points are: $\Gamma = (0, 0, 0)$, $M = (\frac{\pi}{\sqrt{3}}, \frac{\pi}{3})$, $K = (\frac{4\pi}{3\sqrt{3}}, 0)$, $K' = (\frac{2\pi}{3\sqrt{3}}, \frac{2\pi}{3})$.

of the group are:

$$G/T = \{E | \mathbf{0}\}, \{3_{001}^+ | \mathbf{0}\}, \{2_{1-10} | \mathbf{0}\}', \{-1 | \mathbf{0}\} \quad (39)$$

where z corresponds to $[111]$.

Also we define for later use in the exchange coupling matrix the bonds joining nearest neighbors:

$$\delta_x = (0, 1), \quad (40)$$

$$\delta_y = (-\sqrt{3}/2, -1/2), \quad (41)$$

$$\delta_z = (\sqrt{3}/2, -1/2). \quad (42)$$

2. Exchange Hamiltonian

The nearest neighbor model on this lattice has, as symmetry allowed exchange terms, the following on the x , y , z bonds in Eq. 42:

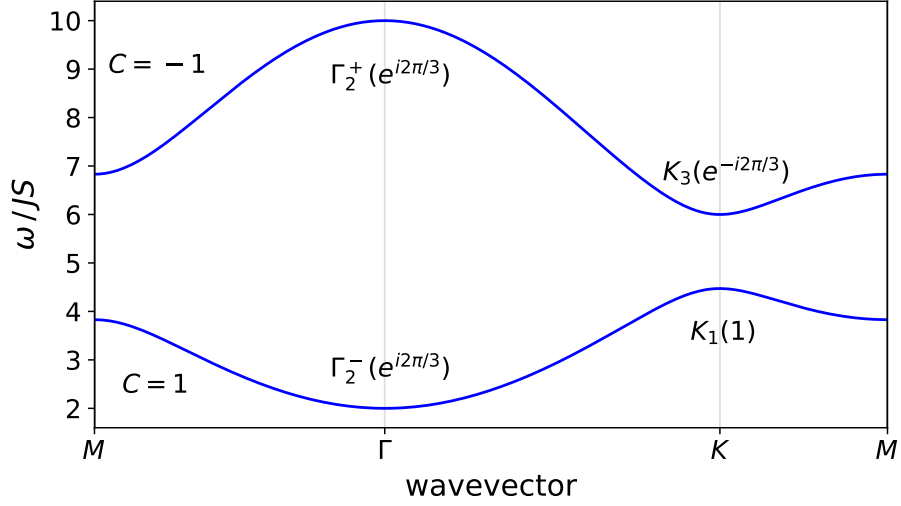


FIG. 4. Dispersion relations of magnons in the honeycomb lattice FM [111] for $J = 0$, $K = 1$ and $h = 5$. At the Γ and K point band representations are indicated with their respective C_3 eigenvalue. The band Chern number is indicated on the left, highlighting the topological gap.

$$J_x = \begin{pmatrix} J + 2K & \Gamma' & \Gamma' \\ \Gamma' & J & \Gamma \\ \Gamma' & \Gamma & J \end{pmatrix} \quad J_y = \begin{pmatrix} J & \Gamma' & \Gamma \\ \Gamma' & J + 2K & \Gamma' \\ \Gamma & \Gamma' & J \end{pmatrix} \quad J_z = \begin{pmatrix} J & \Gamma & \Gamma' \\ \Gamma & J & \Gamma' \\ \Gamma' & \Gamma' & J + 2K \end{pmatrix}. \quad (43)$$

In addition we allow for a magnetic field of magnitude h in the [111] direction. The linear spin wave Hamiltonian approximation is:

$$\mathbf{A}(\mathbf{k}) = \begin{pmatrix} -3J - 2K + h & \left(J + \frac{2K}{3}\right) \left(e^{i\mathbf{k}\cdot\delta_x} + e^{i\mathbf{k}\cdot\delta_y} + e^{i\mathbf{k}\cdot\delta_z}\right) \\ \left(J + \frac{2K}{3}\right) \left(e^{-i\mathbf{k}\cdot\delta_x} + e^{-i\mathbf{k}\cdot\delta_y} + e^{-i\mathbf{k}\cdot\delta_z}\right) & -3J - 2K + h \end{pmatrix} \quad (44)$$

$$\mathbf{B}(\mathbf{k}) = \begin{pmatrix} 0 & \frac{2K}{3} \left(e^{i\mathbf{k}\cdot\delta_x + \frac{2\pi i}{3}} + e^{i\mathbf{k}\cdot\delta_y - \frac{2\pi i}{3}} + e^{i\mathbf{k}\cdot\delta_z}\right) \\ \frac{2K}{3} \left(e^{-i\mathbf{k}\cdot\delta_x + \frac{2\pi i}{3}} + e^{-i\mathbf{k}\cdot\delta_y - \frac{2\pi i}{3}} + e^{-i\mathbf{k}\cdot\delta_z}\right) & 0 \end{pmatrix}. \quad (45)$$

This Hamiltonian contains only the J , K and h couplings. The Γ and Γ' terms merely renormalize the J , K , h model so we have omitted them for simplicity.

3. Band topology

The orbital basis $(J_{\mathbf{q}}^+, J_{\mathbf{q}}^-)$ lives on the Wyckoff position $2c$ with associated site symmetry group generators (here we use the primitive lattice basis):

$$\begin{aligned} \mathbf{q}_1^{2c} = g_1 \mathbf{q}_1^{2c} = (1/3, 2/3) \quad G_{\mathbf{q}_1^{2c}} &= \{3_{001}^+ | 0, 1, 0\}, \{2_{1-10} | 1, 1, 0\}' \\ \mathbf{q}_2^{2c} = g_2 \mathbf{q}_1^{2c} = (2/3, 1/3) \quad G_{\mathbf{q}_2^{2c}} &= \{3_{001}^+ | 1, 1, 0\}, \{2_{1-10} | 1, 1, 0\}' \end{aligned} \quad (46)$$

where we have indicated also the orbit transformations $g_1 = \{E | \mathbf{0}\}$ and $g_2 = \{-1 | 1, 1, 0\}$ forming the coset decomposition $G = \cup_{\alpha} g_{\alpha} (G_{\mathbf{q}_1^{2c}} \times T)$. The group $G_{\mathbf{q}_1^{2c}}$ is therefore isomorphic to $32'$ and the orbitals transform under the representation:

$$\rho_{32'}[(J_{\mathbf{q}}^+, J_{\mathbf{q}}^-)] = {}^1E + {}^2E \quad (47)$$

which induces a two-band decomposable elementary band representation (see Table X). The two bands, once split, produce a topological gap with chiral surface states. The system is a Chern insulator with a bulk invariant associated with a non-trivial Wilson loop that can be computed through the symmetry indicated formulas of the point group C_3 :

$$e^{i\frac{2\pi}{3}C} = \prod_n \Theta_n(\Gamma) \Theta_n(K) \Theta_n(K') \quad (48)$$

where C is the Chern number of the n band(s) and $\Theta(\mathbf{k})$ are the eigenvalues of C_3 . The eigenvalues and irreps of the two bands are:

$$\begin{aligned} \text{band 1 : } \quad \Gamma_2^-(C_3^+) = e^{i\frac{2\pi}{3}}, \quad K_1(C_3^+) = 1, \quad K_1'(C_3^+) = 1 \quad &\rightarrow C = 1 \\ \text{band 2 : } \quad \Gamma_2^+(C_3^+) = e^{i\frac{2\pi}{3}}, \quad K_3(C_3^+) = e^{-i\frac{2\pi}{3}}, \quad K_3'(C_3^+) = e^{-i\frac{2\pi}{3}} \quad &\rightarrow C = -1 \end{aligned} \quad (49)$$

which corresponds to the induced ${}^2E \uparrow G$ band representation (while ${}^1E \uparrow G$ can be found for the negative eigenvalues).

B. Honeycomb XYZ-DM FM [001] model

The honeycomb lattice offers another famous topological gapped model, the Haldane model, which we study here in the context of EBR. The honeycomb isotropic Heisenberg has Dirac cones due to $P\mathcal{T}$ symmetry pinned at K by C_3 . To lift this degeneracy, the spin-space time-reversal symmetry present in Heisenberg need to be broken. This can be achieved either

by having anisotropic Heisenberg (XYZ model) or by introducing a next nearest neighbour DM interaction with out of plane magnetic order (spin wave analog of Haldane model). In both case a gap with non-trivial Chern number will arise. For completeness here we analyze the full model XYZ-DM from an EBR perspective.

1. Crystal structure

The crystal structure we consider is an honeycomb lattice with magnetic moments polarized perpendicular to the honeycomb plane [001]. Both the anisotropic XYZ model and the next NN out of plane DM interaction preserve all the honeycomb symmetry, space group $P6/mmm$. Nevertheless the [001] magnetic order will reduce the group to the type III $P6/mm'm'$ (#191.240). The Wyckoff position is $2c$ with site-symmetry group $-6m'2'$. The generators of the group are:

$$G/T = \{E | \mathbf{0}\}, \{3_{001}^+ | \mathbf{0}\}, \{2_{001} | \mathbf{0}\}, \{2_{1-10} | \mathbf{0}\}', \{-1 | \mathbf{0}\} \quad (50)$$

The primitive lattice and basis are the same as III A. Here we define additionally for later use the bonds joining the next nearest neighbors:

$$\delta_{2x} = (\sqrt{3}, 0), \quad (51)$$

$$\delta_{2y} = (-\sqrt{3}/2, 3/2), \quad (52)$$

$$\delta_{2z} = (-\sqrt{3}/2, -3/2). \quad (53)$$

2. Exchange Hamiltonian

The nearest neighbor anisotropic Heisenberg interaction respect the symmetry of the honeycomb lattice and reads for the x, y, z bonds in Eq. 42:

$$\mathbf{J}_x = \begin{pmatrix} J_x & 0 & 0 \\ 0 & J_y & 0 \\ 0 & 0 & J_z \end{pmatrix} \quad \mathbf{J}_y = \begin{pmatrix} \frac{J_x}{4} + \frac{3J_y}{4} & \frac{\sqrt{3}J_x}{4} - \frac{\sqrt{3}J_y}{4} & 0 \\ \frac{\sqrt{3}J_x}{4} - \frac{\sqrt{3}J_y}{4} & \frac{3J_x}{4} + \frac{J_y}{4} & 0 \\ 0 & 0 & J_z \end{pmatrix} \quad \mathbf{J}_z = \begin{pmatrix} \frac{J_x}{4} + \frac{3J_y}{4} & -\frac{\sqrt{3}J_x}{4} + \frac{\sqrt{3}J_y}{4} & 0 \\ -\frac{\sqrt{3}J_x}{4} + \frac{\sqrt{3}J_y}{4} & \frac{3J_x}{4} + \frac{J_y}{4} & 0 \\ 0 & 0 & J_z \end{pmatrix}. \quad (54)$$

The next nearest neighbor DM interaction has $\mathbf{D} = D\hat{z}$ and exchange hamiltonian for bonds $2x$, $2y$, $2z$ bonds in Eq. 53:

$$\mathbf{J}_{2x} = \mathbf{J}_{2y} = \mathbf{J}_{2z} = \begin{pmatrix} 0 & D & 0 \\ -D & 0 & 0 \\ 0 & 0 & 0 \end{pmatrix} \quad (55)$$

The linear spin wave Hamiltonian approximation is:

$$\mathbf{A}(\mathbf{k}) = \begin{pmatrix} -3J_z + D\gamma(\mathbf{k}) & \left(\frac{J_x+J_y}{2}\right) (e^{i\mathbf{k}\cdot\boldsymbol{\delta}_x} + e^{i\mathbf{k}\cdot\boldsymbol{\delta}_y} + e^{i\mathbf{k}\cdot\boldsymbol{\delta}_z}) \\ \left(\frac{J_x+J_y}{2}\right) (e^{-i\mathbf{k}\cdot\boldsymbol{\delta}_x} + e^{-i\mathbf{k}\cdot\boldsymbol{\delta}_y} + e^{-i\mathbf{k}\cdot\boldsymbol{\delta}_z}) & -3J_z - D\gamma(\mathbf{k}) \end{pmatrix} \quad (56)$$

$$\mathbf{B}(\mathbf{k}) = \begin{pmatrix} 0 & \left(\frac{J_x-J_y}{2}\right) (e^{i\mathbf{k}\cdot\boldsymbol{\delta}_x} + e^{i\mathbf{k}\cdot\boldsymbol{\delta}_y + \frac{2\pi i}{3}} + e^{i\mathbf{k}\cdot\boldsymbol{\delta}_z - \frac{2\pi i}{3}}) \\ \left(\frac{J_x-J_y}{2}\right) (e^{-i\mathbf{k}\cdot\boldsymbol{\delta}_x} + e^{-i\mathbf{k}\cdot\boldsymbol{\delta}_y + \frac{2\pi i}{3}} + e^{-i\mathbf{k}\cdot\boldsymbol{\delta}_z - \frac{2\pi i}{3}}) & 0 \end{pmatrix}. \quad (57)$$

where:

$$\gamma(\mathbf{k}) = \sin(\mathbf{k} \cdot \boldsymbol{\delta}_{2x}) + \sin(\mathbf{k} \cdot \boldsymbol{\delta}_{2y}) + \sin(\mathbf{k} \cdot \boldsymbol{\delta}_{2z}) \quad (58)$$

3. Band topology

The orbital basis ($J_{\mathbf{q}}^+$, $J_{\mathbf{q}}^-$) lives on the Wyckoff position $2c$ with associated site symmetry group generators (here we use the primitive lattice basis):

$$\begin{aligned} \mathbf{q}_1^{2c} = g_1 \mathbf{q}_1^{2c} = (1/3, 2/3) & \quad G_{\mathbf{q}_1^{2c}} = \{3_{001}^+ | 0, 1, 0\}, \{m_{001} | \mathbf{0}\}, \{2_{1-10} | 1, 1, 0\}' \\ \mathbf{q}_2^{2c} = g_2 \mathbf{q}_1^{2c} = (2/3, 1/3) & \quad G_{\mathbf{q}_2^{2c}} = \{3_{001}^+ | 1, 1, 0\}, \{m_{001} | \mathbf{0}\}, \{2_{1-10} | 1, 1, 0\}' \end{aligned} \quad (59)$$

where we have indicated also the orbit transformations $g_1 = \{E | \mathbf{0}\}$ and $g_2 = \{-1 | 1, 1, 0\}$ forming the coset decomposition $G = \cup_{\alpha} g_{\alpha} (G_{\mathbf{q}_1^{2c}} \times T)$. The group $G_{\mathbf{q}_1^{2c}}$ is therefore isomorphic to $-6m'2'$ and the orbitals transform under the representation:

$$\rho_{-6m'2'}[(J_{\mathbf{q}}^+, J_{\mathbf{q}}^-)] = {}^1E'' + {}^2E'' \quad (60)$$

which induces a two-band decomposable elementary band representation (see Table X). The two bands, once split, produce a topological gap with chiral surface states. The system is a Chern insulator with a bulk invariant associated with a non-trivial Wilson loop that can be computed through the symmetry indicated formulas of the point group C_6 :

$$e^{i\frac{2\pi}{6}C} = \prod_n \eta_n(\Gamma) \Theta_n(K) \zeta_n(K') \quad (61)$$

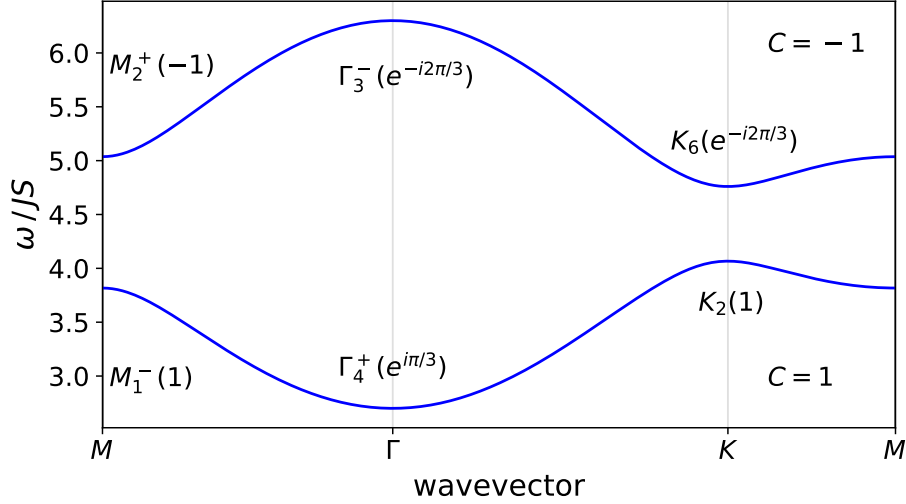


FIG. 5. Dispersion relations of magnons in the honeycomb lattice FM [001] for $J_x = -1$, $J_y = -0.2$, $J_z = -1.5$, $D = 0.1$. At the Γ , K , M points band representations are indicated with their respective C_6 , C_3 , C_2 eigenvalue respectively. The band Chern number is indicated on the right, highlighting the topological gap.

where C is the Chern number of the n band(s) and $\eta(\mathbf{k})$, $\Theta(\mathbf{k})$, $\zeta(\mathbf{k})$ are the eigenvalues of C_6 , C_3 , C_2 . The eigenvalues and irreps of the two bands are:

$$\begin{aligned}
 \text{band 1: } & \Gamma_4^+(C_6^+) = e^{i\frac{\pi}{3}}, K_2(C_3^+) = 1, M_1^-(C_2) = 1 \quad \rightarrow C = 1 \\
 \text{band 2: } & \Gamma_3^-(C_6^+) = e^{-i\frac{2\pi}{3}}, K_6(C_3^+) = e^{-i\frac{2\pi}{3}}, M_2^+(C_2) = -1 \quad \rightarrow C = -1 \quad (62)
 \end{aligned}$$

which corresponds to the induced ${}^2E'' \uparrow G$ band representation (while ${}^1E'' \uparrow G$ can be found for the negative eigenvalues).

C. Stacked honeycomb AFM topological insulator

We now consider a system with AA stacked honeycomb planes with anisotropic couplings within each layer and AFM Heisenberg exchange between layers. This results in a magnonic topological crystalline insulator as noted in [9]. The in-plane model (with decoupled layers) is, from a symmetry perspective, identical to that studied in Sec. III B, which has two split bands with opposite Chern number. Adding a stacked layer with AFM order produces two further bands, but with reversed Chern number. If the two layers are not coupled, the surface state of opposite chiralities survive independently. If the layer are coupled,

for example through AFM Heisenberg, then the respective bulk bands can mix, rendering the Chern invariant ill-defined. Nevertheless the effective anti-unitary symmetry $\mathcal{T}T_{\mathbf{a}_3/2}$ imposes a Kramers degeneracy in the plane $k_z = \pi$, which protects the hybridized surface states from gapping, leading to a topological insulator with a \mathbb{Z}_2 invariant [9].

1. Crystal structure

The crystal structure is a stacked honeycomb lattice with magnetic moments along [001] anti-aligned between layers. In the previous section we have shown how the single layer correspond to group $P6/mm'm'$, but here we have an additional black and white translation between the two AFM layers with magnetic space group type IV P_c6/mcc (#192.252). The Wyckoff position is $4c$ with site-symmetry group $-6m'2'$. The generators of the group are:

$$G/T = \{E | \mathbf{0}\}, \{3_{001}^+ | \mathbf{0}\}, \{2_{001} | \mathbf{0}\}, \{2_{1-10} | 0, 0, 1/2\}, \{-1 | \mathbf{0}\}, \{1 | 0, 0, 1/2\}' \quad (63)$$

The lattice primitive vectors are:

$$\mathbf{a}_1 = (\sqrt{3}/2, 3/2, 0), \quad \mathbf{a}_2 = (\sqrt{3}/2, -3/2, 0), \quad \mathbf{a}_3 = (0, 0, 1) \quad (64)$$

and basis coming from Wyckoff position $4c$ is (origin at the center of the hexagon):

$$\boldsymbol{\delta}_1 = (\sqrt{3}/2, -1/2, 0), \quad \boldsymbol{\delta}_2 = (\sqrt{3}/2, 1/2, 0), \quad \boldsymbol{\delta}_3 = (\sqrt{3}/2, -1/2, 1/2), \quad \boldsymbol{\delta}_4 = (\sqrt{3}/2, 1/2, 1/2) \quad (65)$$

2. Exchange Hamiltonian

The model we consider has exchange

$$J_x S_i^x S_{i+\hat{y}}^x + J_y S_i^y S_{i+\hat{y}}^y + J_z S_i^z S_{i+\hat{y}}^z \quad (66)$$

on the honeycomb bond aligned with y and the components refer to the crystallographic frame with \hat{z} perpendicular to the honeycomb layers. We then tile all bonds using C_3 and translations exactly as in Eq. 54. We coupled the AA layers with a simple AFM Heisenberg J_c coupling. We also include a second-neighbor in-plane Dzyaloshinskii-Moriya coupling considered in Sec. III B, even if not strictly necessary for the non-trivial topology here.

The linear spin wave Hamiltonian is:

$$\mathbf{A}(\mathbf{k}) = \begin{pmatrix} J_H + D \gamma_1(\mathbf{k}) & \left(\frac{J_x+J_y}{2}\right) \gamma_2(\mathbf{k}) & 0 & 0 \\ \left(\frac{J_x+J_y}{2}\right) \gamma_2^*(\mathbf{k}) & J_H - D \gamma_1(\mathbf{k}) & 0 & 0 \\ 0 & 0 & J_H - D \gamma_1(\mathbf{k}) & \left(\frac{J_x+J_y}{2}\right) \gamma_2(\mathbf{k}) \\ 0 & 0 & \left(\frac{J_x+J_y}{2}\right) \gamma_2^*(\mathbf{k}) & J_H + D \gamma_1(\mathbf{k}) \end{pmatrix} \quad (67)$$

$$\mathbf{B}(\mathbf{k}) = \begin{pmatrix} 0 & \left(\frac{J_x-J_y}{2}\right) \beta_1(\mathbf{k}) & -2J_c \cos(\mathbf{k} \cdot \mathbf{a}_3/2) & 0 \\ \left(\frac{J_x-J_y}{2}\right) \beta_1(-\mathbf{k}) & 0 & 0 & -2J_c \cos(\mathbf{k} \cdot \mathbf{a}_3/2) \\ -2J_c \cos(\mathbf{k} \cdot \mathbf{a}_3/2) & 0 & 0 & \left(\frac{J_x-J_y}{2}\right) \beta_1(-\mathbf{k}) \\ 0 & -2J_c \cos(\mathbf{k} \cdot \mathbf{a}_3/2) & \left(\frac{J_x-J_y}{2}\right) \beta_1(\mathbf{k}) & 0 \end{pmatrix}. \quad (68)$$

where:

$$J_H = -3J_z + 2J_c \quad (69)$$

$$\gamma_1(\mathbf{k}) = \sin(\mathbf{k} \cdot \boldsymbol{\delta}_{2x}) + \sin(\mathbf{k} \cdot \boldsymbol{\delta}_{2y}) + \sin(\mathbf{k} \cdot \boldsymbol{\delta}_{2z}) \quad (70)$$

$$\gamma_2(\mathbf{k}) = e^{i\mathbf{k} \cdot \boldsymbol{\delta}_x} + e^{i\mathbf{k} \cdot \boldsymbol{\delta}_y} + e^{i\mathbf{k} \cdot \boldsymbol{\delta}_z} \quad (71)$$

$$\beta_1(\mathbf{k}) = e^{i\mathbf{k} \cdot \boldsymbol{\delta}_x} + e^{i\mathbf{k} \cdot \boldsymbol{\delta}_y + \frac{2\pi i}{3}} + e^{i\mathbf{k} \cdot \boldsymbol{\delta}_z - \frac{2\pi i}{3}} \quad (72)$$

where the x , y , z and $2x$, $2y$, $2z$ bonds are the same as Eq. 42 and Eq. 53 and on all honeycomb layers.

3. Band topology

The orbital basis ($J_{\mathbf{q}}^+$, $J_{\mathbf{q}}^-$) lives on the Wyckoff position $4c$ with associated site symmetry group generators (here we use the primitive lattice basis):

$$\begin{aligned} \mathbf{q}_1^{4c} = g_1 \mathbf{q}_1^{2c} = (1/3, 2/3, 0) & \quad G_{\mathbf{q}_1^{4c}} = \{3_{001}^+ | 0, 1, 0\}, \{m_{001} | \mathbf{0}\}, \{2_{1-10} | 1, 1, 0\}' \\ \mathbf{q}_2^{4c} = g_2 \mathbf{q}_1^{2c} = (2/3, 1/3, 0) & \quad G_{\mathbf{q}_2^{4c}} = \{3_{001}^+ | 1, 1, 0\}, \{m_{001} | \mathbf{0}\}, \{2_{1-10} | 1, 1, 0\}' \end{aligned} \quad (73)$$

$$\begin{aligned} \mathbf{q}_3^{4c} = g_3 \mathbf{q}_1^{2c} = (1/3, 2/3, 1/2) & \quad G_{\mathbf{q}_3^{4c}} = \{3_{001}^+ | 0, 1, 0\}, \{m_{001} | 0, 0, 1\}, \{2_{1-10} | 1, 1, 1\}' \\ \mathbf{q}_4^{4c} = g_4 \mathbf{q}_1^{2c} = (2/3, 1/3, 1/2) & \quad G_{\mathbf{q}_4^{4c}} = \{3_{001}^+ | 1, 1, 0\}, \{m_{001} | 0, 0, 1\}, \{2_{1-10} | 1, 1, 1\}' \end{aligned} \quad (74)$$

where we have indicated also the orbit transformations $g_1 = \{E | \mathbf{0}\}$, $g_2 = \{-1 | 1, 1, 0\}$, $g_3 = \{1 | 0, 0, 1/2\}'$, $g_4 = \{-1 | 1, 1, 1/2\}'$ forming the coset decomposition $G = \cup_{\alpha} g_{\alpha} (G_{\mathbf{q}_1^{4c}} \times T)$.

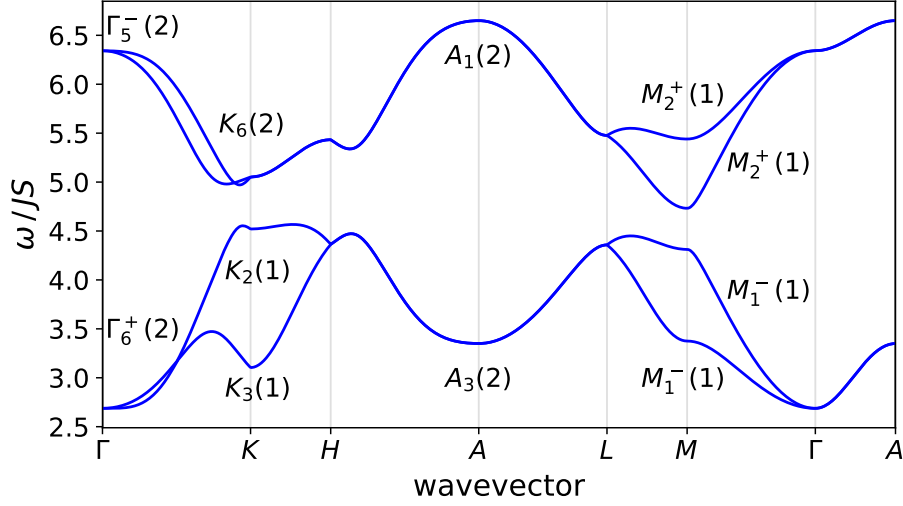


FIG. 6. Dispersion relations of magnons for the AA stacked honeycomb lattice ferromagnet with [001] moments for $J_x = -1$, $J_y = -0.1$, $J_z = -1$, $D = 0.5$, $J_c = -1$. At the Γ , K , M , A points band representations are indicated with their respective dimension. The topological gap comes from the splitting of a 4-band EBR. A nodal surface is present at $[H - A - L]$ and a nodal line along $[\Gamma - A]$.

The group $G_{q_1^{4c}}$ is therefore isomorphic to $-6m'2'$ and the orbitals transform under the representation:

$$\rho_{-6m'2'}[(J_q^+, J_q^-)] = {}^1E'' + {}^2E'' \quad (75)$$

which induces a four-band decomposable elementary band representation (see Table II). The subduced irreps in reciprocal space of the two branches (2 bands each) are:

$$\text{branch 1: } \Gamma_6^+(2), A_3(2), H_3(2), K_3(1) + K_2(1), L_1(2), M_2^-(1) + M_1^-(1)$$

$$\text{branch 2: } \Gamma_5^-(2), A_1(2), H_2(2), K_6(2), L_2(2), M_4^+(1) + M_3^+(1)$$

(76)

which corresponds to the induced ${}^2E'' \uparrow G(4)$ band representation (${}^1E'' \uparrow G(4)$ for negative eigenvalues).

The model has a nontrivial \mathbb{Z}_2 invariant linked to the black and white translation $\{1|0,0,1/2\}'$ [9]. This is indeed reflected by the EBR picture. When the two layers are decoupled, there are two decomposable EBRs ${}^2E'' \uparrow G(2)$ (layer spin up) and ${}^1E'' \uparrow G(2)$ (layer spin down) of the kind in Eq. 62, which produce bands with opposite Chern num-

ber for the opposite layers. When the two layers couple, the black and white translation $\{1|0,0,1/2\}'$ pairs the two EBRs into a new single EBR which is nevertheless decomposable and therefore topological.

Finally the band representation, beside the topological gap, also predicts the nodal plane $E_1E_2(2)$ between each pair of bands.

We have established the topological character of the magnon bands based on symmetry. A more refined analysis reveals that this model has a nontrivial \mathbb{Z}_2 invariant that can be computed from the Berry phase $A_\mu^{(n)}(\mathbf{k})$ in the pairs of bands joined by Kramers degeneracies. Thus for bands $n = 1, 2, 3, 4$ where $n = 1, 2$ form the lower energy pair Ref. [9] show that the relevant invariant is built from $A_\mu^{(-)}(\mathbf{k}) = A_\mu^{(1)}(\mathbf{k}) + A_\mu^{(2)}(\mathbf{k})$ and $A_\mu^{(+)}(\mathbf{k}) = A_\mu^{(3)}(\mathbf{k}) + A_\mu^{(4)}(\mathbf{k})$ and z component of the Berry curvature $F_z^{(\pm)}(\mathbf{k})$

$$\nu^\pm = \frac{1}{2\pi} \left(\oint_{\partial HBZ} dk^\mu A_\mu^{(\pm)}(\mathbf{k}) - \int_{HBZ} d^2k F_z^{(\pm)}(\mathbf{k}) \right) \text{mod } 2 \quad (77)$$

where HBZ refers to half of the zone such that the remainder is covered by $\mathbf{k} \rightarrow -\mathbf{k}$.

EBR	${}^1E'' \uparrow G(4)$	${}^2E'' \uparrow G(4)$
	Decomposable	Decomposable
$\Gamma : (0, 0, 0)$	$\Gamma_5^-(2) + \Gamma_6^+(2)$	$\Gamma_5^-(2) + \Gamma_6^+(2)$
$A : (0, 0, 1/2)$	$A_2(2) + A_4(2)$	$A_1(2) + A_3(2)$
$H : (1/3, 1/3, 1/2)$	$H_1(2) + H_3(2)$	$H_2(2) + H_3(2)$
$K : (1/3, 1/3, 0)$	$K_2(2) + K_3(1) + K_6(2)$	$K_2(2) + K_3(1) + K_6(2)$
$L : (1/2, 0, 1/2)$	$L_1(2) + L_2(2)$	$L_1(2) + L_2(2)$
$M : (1/2, 0, 0)$	$M_1^-(2) + M_2^-(1) + M_3^+(1) + M_4^+(1)$	$M_1^-(2) + M_2^-(1) + M_3^+(1) + M_4^+(1)$
$E : (u, v, 1/2)$	$2E_1E_2(2)$	$2E_1E_2(2)$

TABLE II. Relevant magnon EBR for magnetic space group type IV $Pc6/mcc$ (#192.252) Wyckoff position $4c$ and site symmetry group $-6m'2'$. The table shows the representations subduced at the reciprocal space high symmetry points, with the dimension in the parenthesis. Compatibility relation allow decomposability and therefore a topological gap. In the last line the 2-fold degenerate nodal plane representation.

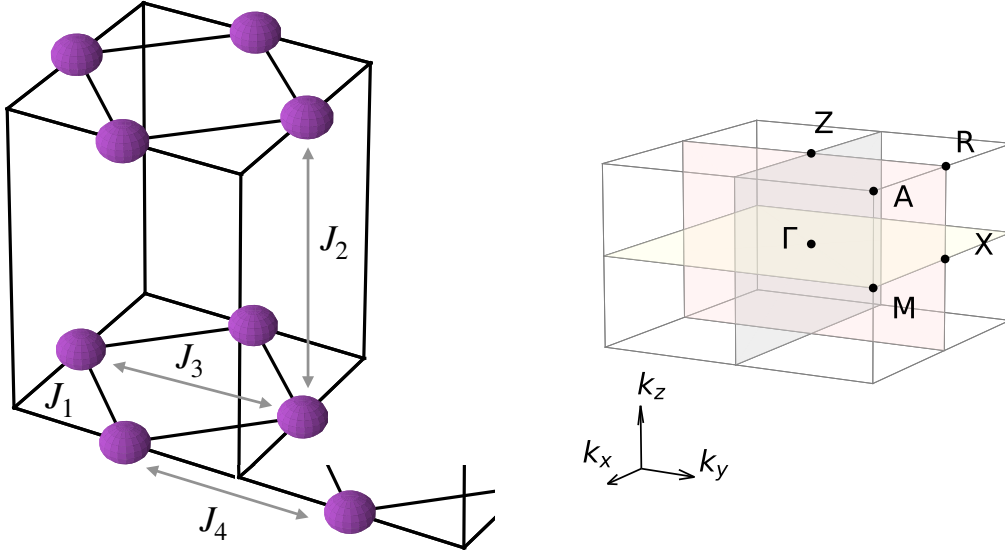


FIG. 7. The lattice of space group $P4$ (#75.1) and its simple tetragonal first Brillouin zone. In the lattice the J_i couplings mentioned in the text are showed. In the Brillouin zone the high symmetry points are: $\Gamma = (0, 0, 0)$, $X = (0, \pi, 0)$, $Z = (0, 0, \pi)$, $M = (\pi, \pi, 0)$, $R = (0, \pi, \pi)$, $A = (\pi, \pi, \pi)$.

D. Space group $P4$; FM [001] model

1. Crystal structure

Here we consider the space group $P4$ (#75.1) with Wyckoff position $2c$. The system is described by a single decomposable EBR with a site-symmetry group C_2 compatible with FM [001] magnetic order and must host a topological gap once the EBR is split.

The lattice is a simple tetragonal with primitive vectors:

$$\mathbf{a}_1 = (a, 0, 0), \quad \mathbf{a}_2 = (0, a, 0), \quad \mathbf{a}_3 = (0, 0, c) \quad (78)$$

The basis coming from Wyckoff position $2c$ is:

$$\boldsymbol{\delta}_1 = (0, 1/2, z), \quad \boldsymbol{\delta}_2 = (1/2, 0, z) \quad (79)$$

The lattice and the first Brillouin zone are shown in Fig. 7.

There are 4 symmetries in the group, all around the axial z direction:

$$G/T = \{E | \mathbf{0}\}, \quad \{2_{001} | \mathbf{0}\}, \quad \{4_{001}^+ | \mathbf{0}\}, \quad \{4_{001}^- | \mathbf{0}\} \quad (80)$$

Also we define for later use in the exchange coupling matrix the additional lattice points:

$$\begin{aligned}\boldsymbol{\delta}_{1x} &= \boldsymbol{\delta}_1 + \mathbf{a}_1, & \boldsymbol{\delta}_{1y} &= \boldsymbol{\delta}_1 + \mathbf{a}_2, & \boldsymbol{\delta}_{1z} &= \boldsymbol{\delta}_1 + \mathbf{a}_3 \\ \boldsymbol{\delta}_{2x} &= \boldsymbol{\delta}_2 + \mathbf{a}_1, & \boldsymbol{\delta}_{2y} &= \boldsymbol{\delta}_2 + \mathbf{a}_2, & \boldsymbol{\delta}_{2z} &= \boldsymbol{\delta}_2 + \mathbf{a}_3\end{aligned}\quad (81)$$

2. Exchange Hamiltonian

The model $J_1 + J_2 + J_3 + J_4$ on this lattice consists of 10 different bond types:

- Set J_1 : $(1, 2)_a, (1, 2)_b, (1, 2)_c, (1, 2)_d$
- Set J_2 : $(1, 1)_z, (2, 2)_z$
- Set J_3 : $(1, 1)_x, (2, 2)_y$
- Set J_4 : $(1, 1)_y, (2, 2)_x$.

Applying the symmetries in Eq. 80 the exchange terms are constrained to 26 possible coupling parameters:

$$\mathbf{J}_{(1,2)_a} = \begin{pmatrix} J_1^{xx} & J_1^{xy} & J_1^{xz} \\ J_1^{yx} & J_1^{yy} & J_1^{yz} \\ J_1^{zx} & J_1^{zy} & J_1^{zz} \end{pmatrix} \quad \mathbf{J}_{(1,2)_b} = \begin{pmatrix} J_1^{yy} & -J_1^{xy} & J_1^{zy} \\ -J_1^{yx} & J_1^{xx} & -J_1^{zx} \\ J_1^{yz} & -J_1^{xz} & J_1^{zz} \end{pmatrix} \quad (82)$$

$$\mathbf{J}_{(1,2)_c} = \begin{pmatrix} J_1^{xx} & J_1^{xy} & -J_1^{xz} \\ J_1^{yx} & J_1^{yy} & -J_1^{yz} \\ -J_1^{zx} & -J_1^{zy} & J_1^{zz} \end{pmatrix} \quad \mathbf{J}_{(1,2)_d} = \begin{pmatrix} J_1^{yy} & -J_1^{xy} & -J_1^{zy} \\ -J_1^{yx} & J_1^{xx} & J_1^{zx} \\ -J_1^{yz} & J_1^{xz} & J_1^{zz} \end{pmatrix} \quad (83)$$

$$\mathbf{J}_{(1,1)_z} = \begin{pmatrix} J_2^{xx} & J_2^{xy} & 0 \\ J_2^{yx} & J_2^{yy} & 0 \\ 0 & 0 & J_2^{zz} \end{pmatrix} \quad \mathbf{J}_{(2,2)_z} = \begin{pmatrix} J_2^{yy} & -J_2^{yx} & 0 \\ -J_2^{xy} & J_2^{xx} & 0 \\ 0 & 0 & J_2^{zz} \end{pmatrix} \quad (84)$$

$$\mathbf{J}_{(1,1)_x} = \begin{pmatrix} J_3^{xx} & J_3^{xy} & J_3^{xz} \\ J_3^{yx} & J_3^{yy} & J_3^{yz} \\ -J_3^{zx} & -J_3^{zy} & J_3^{zz} \end{pmatrix} \quad \mathbf{J}_{(2,2)_y} = \begin{pmatrix} J_3^{yy} & -J_3^{xy} & -J_3^{yz} \\ -J_3^{yx} & J_3^{xx} & J_3^{zx} \\ J_3^{yz} & -J_3^{xz} & J_3^{zz} \end{pmatrix} \quad (85)$$

$$\mathbf{J}_{(1,1)_y} = \begin{pmatrix} J_4^{xx} & J_4^{xy} & J_4^{xz} \\ J_4^{yx} & J_4^{yy} & J_4^{yz} \\ -J_4^{zx} & -J_4^{zy} & J_4^{zz} \end{pmatrix} \quad \mathbf{J}_{(2,2)_x} = \begin{pmatrix} J_4^{yy} & -J_4^{xy} & J_4^{yz} \\ -J_4^{yx} & J_4^{xx} & -J_4^{zx} \\ -J_4^{yz} & J_4^{xz} & J_4^{zz} \end{pmatrix} \quad (86)$$

We consider now a field h polarized state in the [001] direction and apply the LSW approximation obtaining $\mathbf{M}(\mathbf{k})$ with:

$$\begin{aligned}\tilde{J}_{11} = & J_{(1,1)_z} e^{i\mathbf{k}\cdot(\boldsymbol{\delta}_1-\boldsymbol{\delta}_{1z})} + J_{(1,1)_x} e^{i\mathbf{k}\cdot(\boldsymbol{\delta}_1-\boldsymbol{\delta}_{1x})} + J_{(1,1)_y} e^{i\mathbf{k}\cdot(\boldsymbol{\delta}_1-\boldsymbol{\delta}_{1y})} \\ & + J_{(1,1)_z}^T e^{i\mathbf{k}\cdot(\boldsymbol{\delta}_{1z}-\boldsymbol{\delta}_1)} + J_{(1,1)_x}^T e^{i\mathbf{k}\cdot(\boldsymbol{\delta}_{1x}-\boldsymbol{\delta}_1)} + J_{(1,1)_y}^T e^{i\mathbf{k}\cdot(\boldsymbol{\delta}_{1y}-\boldsymbol{\delta}_1)}\end{aligned}\quad (87)$$

$$\begin{aligned}\tilde{J}_{22} = & J_{(2,2)_z} e^{i\mathbf{k}\cdot(\boldsymbol{\delta}_2-\boldsymbol{\delta}_{2z})} + J_{(2,2)_x} e^{i\mathbf{k}\cdot(\boldsymbol{\delta}_2-\boldsymbol{\delta}_{2x})} + J_{(2,2)_y} e^{i\mathbf{k}\cdot(\boldsymbol{\delta}_2-\boldsymbol{\delta}_{2y})} \\ & + J_{(2,2)_z}^T e^{i\mathbf{k}\cdot(\boldsymbol{\delta}_{2z}-\boldsymbol{\delta}_2)} + J_{(2,2)_x}^T e^{i\mathbf{k}\cdot(\boldsymbol{\delta}_{2x}-\boldsymbol{\delta}_2)} + J_{(2,2)_y}^T e^{i\mathbf{k}\cdot(\boldsymbol{\delta}_{2y}-\boldsymbol{\delta}_2)}\end{aligned}\quad (88)$$

$$\tilde{J}_{12} = J_{(1,2)_a} e^{i\mathbf{k}\cdot(\boldsymbol{\delta}_1-\boldsymbol{\delta}_2)} + J_{(1,2)_b} e^{i\mathbf{k}\cdot(\boldsymbol{\delta}_1-\boldsymbol{\delta}_{2y})} + J_{(1,2)_c} e^{i\mathbf{k}\cdot(\boldsymbol{\delta}_{1x}-\boldsymbol{\delta}_{2y})} + J_{(1,2)_d} e^{i\mathbf{k}\cdot(\boldsymbol{\delta}_{1x}-\boldsymbol{\delta}_2)}\quad (89)$$

$$\tilde{J}_{21} = J_{(1,2)_a}^T e^{i\mathbf{k}\cdot(\boldsymbol{\delta}_2-\boldsymbol{\delta}_1)} + J_{(1,2)_b}^T e^{i\mathbf{k}\cdot(\boldsymbol{\delta}_{2y}-\boldsymbol{\delta}_1)} + J_{(1,2)_c}^T e^{i\mathbf{k}\cdot(\boldsymbol{\delta}_{2y}-\boldsymbol{\delta}_{1x})} + J_{(1,2)_d}^T e^{i\mathbf{k}\cdot(\boldsymbol{\delta}_2-\boldsymbol{\delta}_{1x})}\quad (90)$$

in Eqs. 17 and 18.

3. Band topology

The orbital basis $(J_{\mathbf{q}}^+, J_{\mathbf{q}}^-)$ sits here on the Wyckoff position $2c$ with associated site symmetry group:

$$\begin{aligned}\mathbf{q}_1^{2c} = g_1 \mathbf{q}_1^{2c} &= (0, 1/2, z) & G_{\mathbf{q}_1^{2c}} &= \{2_{001} | 0, 1, 0\} \\ \mathbf{q}_2^{2c} = g_2 \mathbf{q}_1^{2c} &= (1/2, 0, z) & G_{\mathbf{q}_2^{2c}} &= \{2_{001} | 1, 0, 0\}\end{aligned}\quad (91)$$

where we have indicated also the orbit transformations $g_1 = \{E | \mathbf{0}\}$ and $g_2 = \{4_{001}^- | \mathbf{0}\}$ forming the coset decomposition $G = \bigcup_{\alpha} g_{\alpha} (G_{\mathbf{q}_1^{2c}} \times T)$. The group $G_{\mathbf{q}_1^{2c}}$ is therefore isomorphic to C_2 and the orbital have representation:

$$\rho_{C_2}[(J_{\mathbf{q}}^+, J_{\mathbf{q}}^-)] = 2B\quad (92)$$

which induce a two-bands decomposable elementary band representation (see Table III). The two bands once splitted produced a topological gap with chiral surface states. Indeed the system is a Chern insulator with a bulk invariant associated with a non-trivial Wilson loop that can be computed through the symmetry indicated formulas of the point group C_4 :

$$i^C = \prod_n \xi_n(\Gamma) \xi_n(M) \zeta_n(X)\quad (93)$$

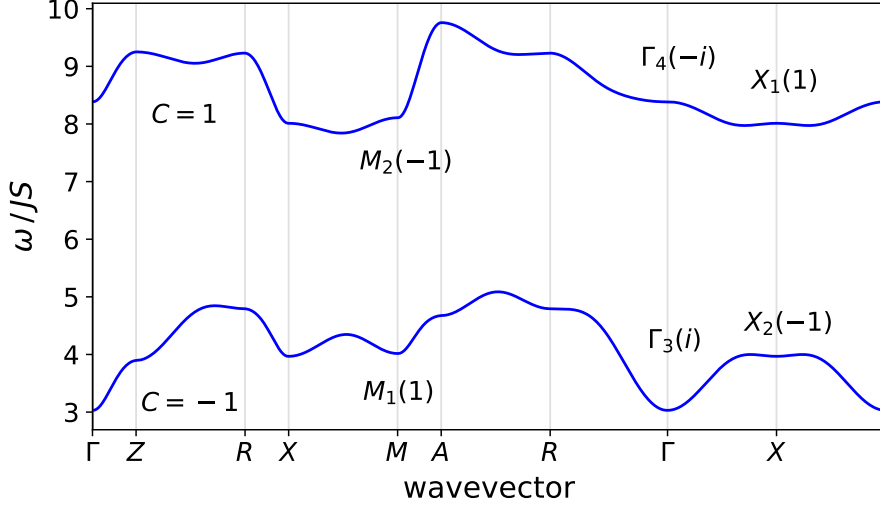


FIG. 8. Dispersion relations of magnons in the space group $P4$ (#75.1) FM [001] lattice for random strong SO couplings $J_1 + J_2 + J_3 + J_4$ and $h = 5$. At the Γ , M and X point band representations are indicated with their respective C_4 or C_2 eigenvalue. The band Chern number is indicated on the left, highlighting the topological gap.

where C is the Chern number of the n band(s), while $\xi(\mathbf{k})$ and $\zeta(\mathbf{k})$ are the eigenvalues respectively of C_4 and C_2 . The eigenvalues and irreps of the two bands are:

$$\begin{aligned}
 \text{band 1 : } & \Gamma_3(C_4^+) = i, M_1(C_4^+) = 1, X_2(C_2) = -1 \quad \rightarrow C = -1 \\
 \text{band 2 : } & \Gamma_4(C_4^+) = -i, M_2(C_4^+) = -1, X_1(C_2) = 1 \quad \rightarrow C = 1
 \end{aligned} \tag{94}$$

which corresponds to the induced $B \uparrow G$ band representation.

IV. NODAL TOPOLOGY IN MAGNONS

EBRs are also useful in determining the nodal topology of a given magnetic space group. While different EBRs can accidentally cross each other, degeneracies cannot be enforced between them. The only symmetry enforced degeneracies are inside EBRs themselves. For magnons, all the single-valued EBRs are relevant, although only a subset can be directly induced as single EBR (due to compatibility with magnetic order). Those that cannot be induced in this way must be induced from lower symmetric Wyckoff positions as components of a composite of EBRs.

In Tab. IV the total number of single-valued EBRs with enforced degeneracy is given with

EBR	$B \uparrow G(2)$
	Decomposable
$\Gamma : (0, 0, 0)$	$\Gamma_3(1) + \Gamma_4(1)$
$A : (1/2, 1/2, 1/2)$	$A_1(1) + A_2(1)$
$M : (1/2, 1/2, 0)$	$M_1(1) + M_2(1)$
$R : (0, 1/2, 1/2)$	$R_1(1) + R_2(1)$
$X : (0, 1/2, 0)$	$X_1(1) + X_2(1)$
$Z : (0, 0, 1/2)$	$Z_3(1) + Z_4(1)$

TABLE III. Relevant magnon EBR for space group $P4$ (#75.1) Wyckoff position $2c$ and site symmetry group 2. The table shows the representations subduced at the reciprocal space high symmetry points, with the dimension in the parenthesis. Compatibility relation allow decomposability and therefore a topological gap.

rows indicating the nature of the degeneracy (point, line or plane) and columns giving the order of the degeneracy. Evidently, symmetry-enforced 2-fold degenerate points are rather common among all EBRs. In addition, 3, 4 and 6-fold points can arise even among the singled-valued groups. A greater diversity of nodal topology is possible in the double magnetic groups that are important in spin-orbit coupled electronic systems but not generically for magnons. In addition to point-like degeneracies, we have listed the number of nodal lines and surfaces appearing among the single-valued EBRs.

The complete set of symmetry data required to obtain the various types of nodal topology can be found on the Bilbao Crystallographic Server [1, 2]. For convenience we provide tabulation of the the magnetic space group and Wyckoff positions relevant to magnons that enforce the more exotic nodal features:

- Nodal point 6-fold in Tab. V.
- Nodal point 4-fold in Tab. VIII.
- Nodal point 3-fold in Tab. VII.
- Nodal lines 4-fold in Tab. VI.
- Nodal plane 2-fold in Tab. IX.

Here we mention that if we relax the locking between spin and space and we deal with spin-space groups, generally the degeneracies present in the system are much higher, producing more exotic nodal features which are not possible in magnetic space groups.

Nodal	2	3	4	5	6
Point	16414	1621	3444	/	289
Line	14151	/	462	/	/
Plane	5442	/	/	/	/

TABLE IV. Statistics of nodal features for single-valued EBRs. In total the single-valued EBRs are 20,206. The rows indicated the reciprocal space dimension: high symmetry points, lines and planes. The columns are the order of degeneracy of the nodal feature and the values listed are the number of different single-valued EBRs. The high symmetric nodal points (lines) embedded in a nodal line (surface) are included in the table.

A. Nodal Topology: Pyrochlore AIAO Order

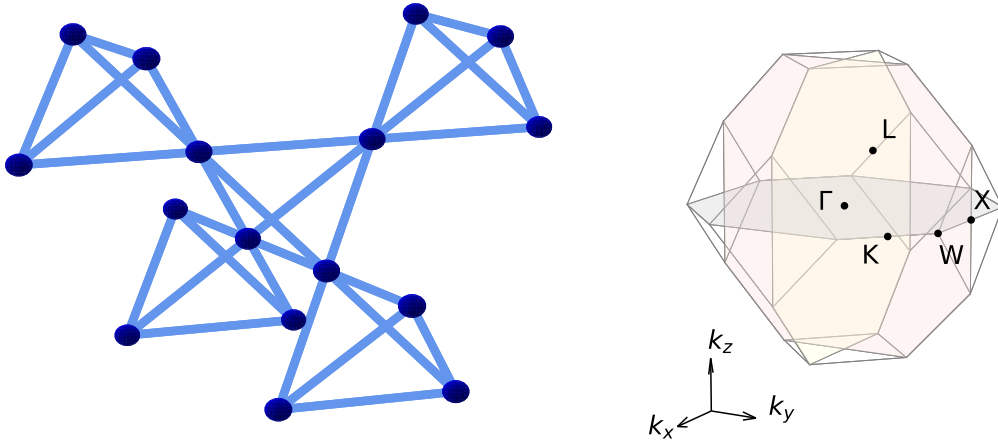


FIG. 9. The pyrochlore lattice and its first Brillouin Zone (space group $Fd\bar{3}m$ #227). In the Brillouin zone the position of the high symmetry points are: $\Gamma = (0, 0, 0)$, $X = (0, 2\pi, 0)$, $L = (\pi, \pi, \pi)$, $W = (\pi, 2\pi, 0)$, $K = (\frac{3\pi}{2}, \frac{3\pi}{2}, 0)$.

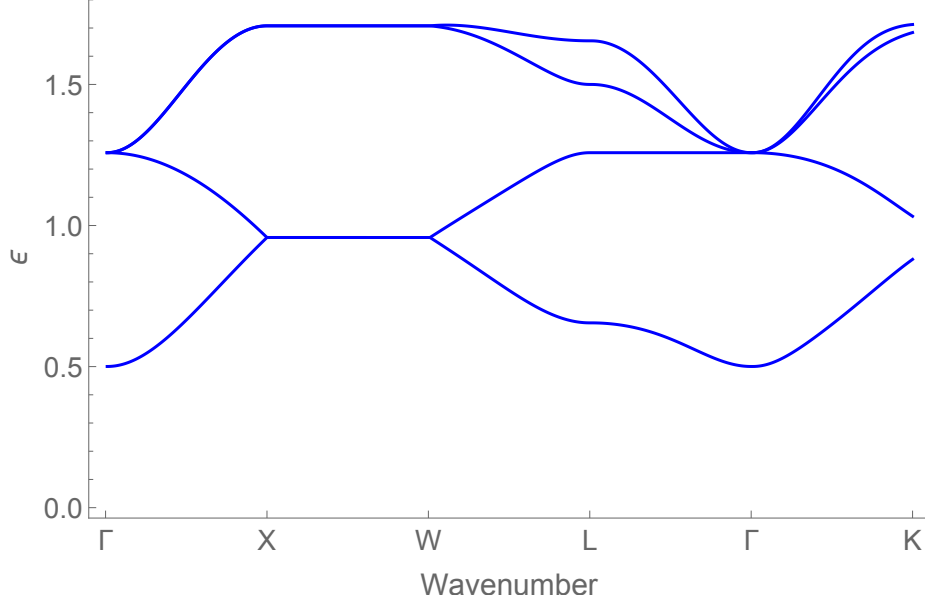


FIG. 10. Dispersion relations of magnons in the pyrochlore lattice AIAO phase for $J = 1$ and $K = -1/6$. There is a three-fold degenerate point in the upper three bands at Γ as well as two two-fold degenerate lines along XW and one nodal line $\Gamma - X$.

As an example of a 3-fold degeneracy we consider the case of the pyrochlore antiferromagnet with all-in/all-out (AIAO) magnetic order. The pyrochlore lattice is a lattice of corner-sharing tetrahedra and the AIAO order has propagation vector $\mathbf{k} = 0$ with moments pointing into or out from the tetrahedral centers. A simple model leading to this magnetic order is the nearest neighbor antiferromagnetic Heisenberg coupling and the symmetry-allowed nearest neighbor Ising exchange

$$H = \sum_{\langle ia,jb \rangle} J \mathbf{S}_{ia} \cdot \mathbf{S}_{jb} + K (\mathbf{S}_{ia} \cdot \hat{\mathbf{z}}_a) (\mathbf{S}_{jb} \cdot \hat{\mathbf{z}}_b) \quad (95)$$

where i, j are primitive fcc sites and a, b are tetrahedral sublattice indices, $\hat{\mathbf{z}}_a$ is the local $\langle 111 \rangle$ direction on sublattice a and $J > 0$, $K < 0$.

The magnetic order breaks down the paramagnetic symmetries to a type III magnetic space group, 227.131 (BNS) that retains the C_3 and C_2 symmetries of the original lattice but the 2-fold screw about $[110]$ chains and S_4 about $[001]$ survive only in combination with a time reversal operation. These symmetries enforce a 3-fold degenerate point at Γ that is shown in Fig. 10 [10].

B. Nodal Topology: Garnet Structure

The table of six-fold degenerate points reveals such a symmetry-enforce point for magnetic space group 230.148 with magnetic structure on the 24c Wyckoff positions. The lattice is a BCC Bravais lattice with a 12 site basis. $(0,0,0) + (1/2,1/2,1/2) +$

$$\begin{array}{cccc} (1/8, 0, 1/4) & (3/8, 0, 3/4) & (1/4, 1/8, 0) & (3/4, 3/8, 0) \\ (0, 1/4, 1/8) & (0, 3/4, 3/8) & (7/8, 0, 3/4) & (5/8, 0, 1/4) \\ (3/4, 7/8, 0) & (1/4, 5/8, 0) & (0, 3/4, 7/8) & (0, 1/4, 5/8). \end{array}$$

This structure arises in the garnets with formula $R_3M_5O_{12}$ on the R sites. The site symmetry of the 230 space group at 24c consists of three C_2 rotations at each site. The magnetic structure compatible with 230.148 is shown in Fig. 2 in the main text. This structure arises in $Dy_3Al_5O_{12}$.

To compute spin waves for this structure with the requisite symmetries, we should include all symmetry-allowed exchange couplings. To nearest neighbor the 24 sites split into two independent sublattices of corner sharing triangles – the garnet hyperkagome. The fact that some C_2 rotations leave bonds invariant constrains the type of exchange couplings. In the absence of symmetry, there are nine possible couplings per bond. The C_2 rotations mix the bonds within each sublattice. This means that the bonds are equivalent and by fixing the interactions on a single bond we may generate the interactions on an entire sublattice. One may show that there are six allowed couplings to nearest neighbor. These are:

$$\begin{array}{l} (1) \quad S_i^y S_j^y \\ (2) \quad S_i^x S_j^x + S_i^z S_j^z \\ (3) \quad S_i^x S_j^z \\ (4) \quad S_i^z S_j^x \\ (5) \quad S_i^z S_j^y + S_i^y S_j^x \\ (6) \quad S_i^x S_j^y + S_i^y S_j^z \end{array}$$

on the bond joining sites $(1/8, 0, 1/4)$ and $(0, 1/4, 1/8)$. The third of these couplings is an effective Ising coupling that fixes the required magnetic structure up to time reversal on the decoupled sublattice. The structure is stable to small additional couplings and we further include a Heisenberg exchange between the two sublattices.

For a model with the J_3 nearest neighbor coupling, antiferromagnetic Heisenberg exchange between nearest neighbors and small additional nearest neighbor couplings, we compute the linear spin wave spectrum. The spectrum along various high symmetry paths is shown in Fig. 2 in the main text. Symmetry predicts the following pattern of degeneracies

$$\Gamma = 3, 3, 3, 3$$

$$H(1, 1, 1) = 2, 2, 2, 6$$

$$N(1/2, 1/2, 0) = 2, 2, 2, 2, 2, 2$$

$$P(1/2, 1/2, 1/2) = 2, 2, 2, 2, 2, 2$$

$$\Delta(0, v, 0) = 1, 1, 1, 1, 2, 2, 2, 2$$

$$G(1 + u, 1 - u, 1) = 2, 2, 2, 2, 2, 2$$

and these are confirmed by direct calculation for the aforementioned couplings. Note the presence of a six-fold degenerate point at H on the zone boundary which is protected by non-symmorphic symmetries and which is clearly visible in the figure. This point is linearly dispersing and can be thought of as a doubled spin-one Weyl point. The 3-fold degenerate points at Γ by contrast are forced to have quadratic dispersion by the inversion symmetry of the lattice.

-
- [1] M. I. Aroyo, J. M. Perez-Mato, C. Capillas, E. Kroumova, S. Ivantchev, G. Madariaga, A. Kirov, and H. Wondratschek, Bilbao crystallographic server: I. databases and crystallographic computing programs, *Zeitschrift für Kristallographie - Crystalline Materials* **221**, 15 (2006).
 - [2] M. I. Aroyo, A. Kirov, C. Capillas, J. M. Perez-Mato, and H. Wondratschek, Bilbao Crystallographic Server. II. Representations of crystallographic point groups and space groups, *Acta Crystallographica Section A* **62**, 115 (2006).
 - [3] A. Corticelli, R. Moessner, and P. A. McClarty, Spin-space groups and magnon band topology, *Physical Review B* **105**, 10.1103/physrevb.105.064430 (2022).
 - [4] C. Bradley and A. Cracknell, *The mathematical theory of symmetry in solids: representation theory for point groups and space groups* (Oxford University Press, 2009).

- [5] L. Elcoro, B. J. Wieder, Z. Song, Y. Xu, B. Bradlyn, and B. A. Bernevig, Magnetic topological quantum chemistry (2020), arXiv:2010.00598 [cond-mat.mes-hall].
- [6] Y. Xu, L. Elcoro, Z.-D. Song, B. J. Wieder, M. G. Vergniory, N. Regnault, Y. Chen, C. Felser, and B. A. Bernevig, High-throughput calculations of magnetic topological materials, *Nature* **586**, 702–707 (2020).
- [7] P. A. McClarty, X.-Y. Dong, M. Gohlke, J. G. Rau, F. Pollmann, R. Moessner, and K. Penc, Topological magnons in Kitaev magnets at high fields, *Phys. Rev. B* **98**, 060404 (2018).
- [8] D. G. Joshi, Topological excitations in the ferromagnetic Kitaev-Heisenberg model, *Phys. Rev. B* **98**, 060405 (2018).
- [9] H. Kondo and Y. Akagi, Dirac surface states in magnonic analogs of topological crystalline insulators, *Phys. Rev. Lett.* **127**, 177201 (2021).
- [10] S.-K. Jian and W. Nie, Weyl magnons in pyrochlore antiferromagnets with an all-in-all-out order, *Phys. Rev. B* **97**, 115162 (2018).

MSGs	MWP	MSGs	MWP	MSGs	MWP	MSGs	MWP	MSGs	MWP
195.3		218.82	II	221.97		223.104		224.115	
200.17		218.83		222.98	12d, 8c	223.105	II	230.145	24d, 16a
201.21	8c	218.84	12d	222.99	II	223.107	8e	230.146	II
207.43	12d, 8c	220.90	II	222.101	8c	223.108		230.148	24c, 16b, 16a
208.47		220.91	16c	222.102		223.109		230.149	
215.73				222.103	12d, 8c				

TABLE V. List of all single-valued magnetic space group (type I,II,III,IV) with 6-fold high symmetry points, therefore all possible cases in magnons. The first column (MSGs) uses the BNS convention for the magnetic space group. The second (MWP) indicates the maximal Wyckoff position, if the magnon degenerate EBR is directly deducible from it (compatibility with magnetic order). If blank space then the degenerate EBR can only be induced in a composite magnon BR from a lower symmetric Wyckoff position. The type *II* group with pure time-reversal are also listed for completeness, signed with *II*, but they are not relevant for ordered magnonic systems with strong spin-orbit as considered in this paper.

MSGs	MWP	MSGs	MWP	MSGs	MWP	MSGs	MWP	MSGs	MWP
49.274	4c, 4d, 4g	53.331	4b, 4a, 8g	57.390	8c, 8e	60.429	8c, 8e	125.374	8e
49.276	4c, 4d	53.335	4b, 4a, 8e	58.401	4c, 4a	61.434	II	128.408	4d, 4a
50.286	8d, 8h	53.336	4b, 4a, 4e	58.402	4c, 4b, 4a	61.435		129.420	8d
50.288	8e	54.349	8c, 8e	59.413	8c	61.438	8c, 8d, 8b	132.458	
51.300	4b, 4a	54.352	8c, 8d, 8a, 8e	59.414	8d	62.442	II	133.470	8e
51.301	4b, 4a	57.378	II	60.418	II	62.445	4c	136.504	
52.316	8c, 8d, 8a, 8e	57.379	4c, 4d	60.420	4c	62.452	8c, 8d, 8b	137.516	8d
52.318	4c, 8d	57.386	8c, 8d, 8a	60.427	8c, 8d, 8a	124.362	4c, 4d	205.34	II
53.330	4c, 4a, 4f, 4e								

TABLE VI. List of all single-valued magnetic space group (type I,II,III,IV) with 4-fold high symmetry lines, therefore all possible cases in magnons. The first column (MSGs) uses the BNS convention for the magnetic space group. The second (MWP) indicates the maximal Wyckoff position, if the magnon degenerate EBR is directly deducible from it (compatibility with magnetic order). If blank space then the degenerate EBR can only be induced in a composite magnon BR from a lower symmetric Wyckoff position. The type *II* group with pure time-reversal are also listed for completeness, signed with *II*, but they are not relevant for ordered magnonic systems with strong spin-orbit as considered in this paper.

MSGs	MWP	MSGs	MWP	MSGs	MWP	MSGs	MWP
195.1		206.39	24d	216.76		224.113	4c, 4b, 12f
195.2	II	207.40		216.77		224.114	
195.3		207.41	II	217.78	12d	224.115	
196.4		207.42		217.79	II	225.116	
196.5	II	207.43	8c, 12d	217.80		225.117	II
196.6	24c, 24d	208.44		218.81	6c, 6d	225.118	
197.7		208.45	II	218.82	II	225.119	24d
197.8	II	208.46	4c, 4b, 6e, 6f	218.83		225.120	
198.9	4a	208.47		218.84	12d	225.121	
198.10	II	209.48		219.85	24c, 24d	226.122	24d
198.11	12b, 8a	209.49	II	219.86	II	226.123	II
199.12	12b, 8a	209.50	24d	219.87		226.124	24c
199.13	II	209.51	24d	219.88	24c, 24d	226.125	
200.14		210.52		220.89	12a, 12b, 16c	226.126	
200.15	II	210.53	II	220.90	II	226.127	24c
200.16		210.54	16d, 16c	220.91	16c	227.128	
200.17		210.55	48d, 32c, 48f, 48e	221.92		227.129	II
201.18	4c, 4b	211.56		221.93	II	227.130	
201.19	II	211.57	II	221.94		227.131	16d, 16c
201.20		211.58	8c, 12d	221.95		227.132	
201.21	8c	212.59		221.96		227.133	96f
202.22	24d	212.60	II	221.97		228.134	48d, 32c
202.23	II	212.61	4b, 4a	222.98	8c, 12d	228.135	II
202.24		212.62	8b, 12d, 12c	222.99	II	228.136	32b, 48d
202.25	24c	213.63		222.100	12d	228.137	32b, 32c
203.26	16d, 16c	213.64	II	222.101	8c	228.138	
203.27	II	213.65	4b, 4a	222.102		228.139	32b, 48d, 96f
203.28		213.66	12d, 12c, 8a	222.103	8c, 12d	229.140	
203.29	32b, 48d	214.67		223.104		229.141	II
204.30	8c	214.68	II	223.105	II	229.142	12d
204.31	II	214.69	12d, 8b, 12c, 8a	223.106	8e, 6c, 6d	229.143	8c
204.32		215.70		223.107	8e	229.144	
205.33	4b, 4a	215.71	II	223.108		230.145	24d, 16a
205.34	II	215.72		223.109		230.146	II
205.35		215.73		224.110		230.147	24c, 24d, 16b
205.36	24d, 8b	216.74		224.111	II	230.148	24c, 16b, 16a
206.37	24d, 8b, 8a	216.75	II	224.112	12f	230.149	
206.38	II						

TABLE VII. List of all single-valued magnetic space group (type I,II,III,IV) with 3-fold high symmetry points, therefore all possible cases in magnons. The first column (MSGs) uses the BNS convention for the magnetic space group. The second (MWP) indicates the maximal Wyckoff position, if the magnon degenerate EBR is directly deducible from it (compatibility with magnetic order). If blank space then the degenerate EBR can only be induced in a composite magnon BR from a lower symmetric Wyckoff position. The type *II* group with pure time-reversal are also listed for completeness, signed with *II*, but they are not relevant for ordered magnonic systems with strong spin-orbit as considered in this paper.

TABLE VIII: List of all single-valued magnetic space group (type I,II,III,IV) with 4-fold high symmetry points, therefore all possible cases in strong SO magnons. The first column (MSGs) uses the BNS convention for the magnetic space group. The second (MWP) indicates the maximal Wyckoff position, if the magnon degenerate EBR is directly deducible from it (compatibility with magnetic order). If blank space then the degenerate EBR can only be induced in a composite magnon BR from a lower symmetric Wyckoff position. The type *II* group with pure time-reversal are also listed for completeness, signed with *II*, but they are not relevant for ordered magnonic systems with strong spin-orbit as considered in this paper.

MSGs	MWP	MSGs	MWP	MSGs	MWP	MSGs	MWP
11.55	4c, 4a, 4e	56.374	4b, 4a, 8e	110.246	II	141.560	16d, 16e, 16c
13.71	4d, 4a, 4f, 4e	57.378	II	110.247	8a	142.562	II
13.74	4b, 4a, 4e	57.379	4c, 4d	111.256	4f	142.564	16e, 16c
14.80	4c, 4a	57.382	4c, 4b, 4a, 4d	111.258		142.566	8b, 16e, 8a
17.11	4c, 4b, 4a, 4d	57.383	4c, 4b, 4a, 4d	112.265	8i	142.569	16e
17.14	4b, 4a	57.386	8c, 8d, 8a	112.266		156.52	
17.15	4c, 4b, 4a	57.387	4c, 4d, 4f, 4e	113.272	4a	157.56	4b
18.21	4b, 4a	57.390	8c, 8e	113.274	4c, 4d	158.58	II
18.22	4b, 4a	57.391	4c, 8d	114.276	II	159.62	II
19.26	II	57.392	4b, 4a, 8e	114.280	4c, 4b	160.68	
19.28	4b, 4a	58.400	4c, 4d, 8g	115.288		161.70	II
28.93	4c, 4b, 4a	58.401	4c, 4a	115.290		162.78	4d, 6f
28.94	4c, 4b, 4a	58.402	4c, 4b, 4a	116.298	4d	163.80	II
28.95	4b, 4a	58.403	4c, 4b, 4a, 4d	117.304	4d, 4a	163.82	
28.96	4c, 4b, 4a	59.412	4d, 4b, 4f	117.306	4b, 4a	164.90	6e
28.98	4b, 4a	59.413	8c	118.312	4d, 4b	165.92	II
29.100	II	59.414	8d	118.313	4c, 4b, 4d, 4f	165.94	4d
29.104	4b, 4a	60.418	II	123.348		166.102	18e
29.105	8a	60.420	4c	123.350		167.104	II
29.107	4a	60.422	4c, 4b, 4a	124.352	II	167.106	
29.109	4a	60.423	4c, 4b, 4a	124.354	4f, 4e	176.144	II
29.110	4b, 4a	60.424	4c, 4b, 4a	124.355	4e	176.148	4c, 6g
30.116	4b, 4a	60.425	4c	124.359		183.190	
30.117	4c, 4b, 4a, 4d	60.426	8c, 8d, 8b, 8e	124.361	4b, 8f	184.192	II
30.118	4c, 4b, 4a	60.427	8c, 8d, 8a	124.362	4c, 4d	184.193	4b, 6c
30.120	4a	60.428	4c, 4d, 8g	125.372	4b, 8e	184.194	4b, 6c
30.121	4c, 4b, 4a	60.429	8c, 8e	125.374	8e	185.198	II

TABLE VIII – *Continued from previous page*

MSGs	MWP	MSGs	MWP	MSGs	MWP	MSGs	MWP
30.122	4b, 4a	60.430	4b, 4a, 8h, 8c	126.376	II	185.199	4b
31.128	4b, 4a	60.431	4c, 4b, 4a	126.378	4c, 8f	185.202	4b, 6c
31.129	4a	60.432	4c, 4b, 4a, 4d	126.379	8f	186.204	II
31.130	4c, 4b, 4a	61.434	II	126.383		186.206	
31.131	4b, 4a	61.435		126.384	4c, 8e, 4a	186.208	6c
31.133	4a	61.436	4b, 4a	126.385	8e, 8f	187.214	
32.139	4b, 4a	61.437		126.386	8f	188.216	II
32.142	4a	61.438	8c, 8d, 8b	127.396	4a	188.217	
32.143	4b, 4a	61.439	4b, 4a, 8e	127.398	4c, 4a	189.226	4c
33.145	II	61.440	8c, 8d, 8b, 8e	128.400	II	190.228	II
33.149	4a	62.442	II	128.402	4c	190.230	
33.150	8a	62.445	4c	128.403	4c, 4d	191.242	
33.151	4b, 4a	62.446	4c, 4b, 4a	128.406		192.244	II
33.153	4a	62.447	4c, 4b, 4a	128.407		192.246	4c, 4d, 6f
33.154	4a	62.448	4c, 4b, 4a	128.408	4d, 4a	192.247	4d, 6f
34.160	4b, 4a	62.450	4b, 4a, 8d	128.409	4c, 4d, 8f	192.248	6g, 6f
34.161	4b, 4a	62.451	4d, 4b	129.420	8d	192.249	4c, 6g, 6f
34.162	4b, 4a	62.452	8c, 8d, 8b	129.422	8f	192.251	
34.163	4c, 4b, 4a	62.454	4c, 4b, 4a	130.424	II	193.253	4c, 6f
48.262	4b, 4a, 8e	62.455	8c, 8e	130.426	8d	193.254	II
48.263	4f, 4e	63.467	8d, 8a, 8f	130.427	4a, 8d	193.256	4c, 4d
49.272	4c, 4a, 4f, 4h	67.508	8c, 8e, 8b	130.428	4b, 4a	193.258	6f
49.274	4c, 4d, 4g	68.518	8c, 8e, 8g, 8a	130.429	4c, 4b, 4a, 8d	193.261	
49.275	4c, 4d	73.549	II	130.430		193.262	4c, 6g
49.276	4c, 4d	73.552	8c, 8d, 8e	130.431	4c	194.263	6g
50.284	4d, 4b, 4f, 4h	74.561	8e, 8d, 8b, 8a	130.432	4c, 4a, 8d	194.264	II
50.285	4c, 8e, 4d	84.56	4e	130.433	8e, 4a, 8f	194.267	
50.286	8d, 8h	84.58	4c, 4d	130.434	8e, 4a	194.269	6g
50.288	8e	85.64	4c, 4a, 8d	131.444		194.271	
51.299	4c, 4a, 4f	85.66	8f	131.445	8e	194.272	6g
51.300	4b, 4a	86.72	4b, 8d	131.446		198.10	II
51.301	4b, 4a	86.74	8f	132.456	4f	198.11	12b, 8a
51.303	4b, 4a, 4f, 4e	89.94		132.457	4b	205.34	II
51.304	4b, 4a	90.100	4c, 4b	132.458		205.35	
52.306	II	91.109	8c, 8b, 8a	133.460	II	205.36	24d, 8b
52.310	4c, 4b, 4a, 4d	91.110	4b, 4a, 8f	133.462	4b, 8e	206.38	II
52.311	4c, 4b, 4a, 4d	92.112	II	133.463	8e	206.39	24d
52.313	4c, 4d	92.115	4a	133.467		212.59	
52.314	4b, 4a, 8g	92.116	4b, 4a, 8d	133.468	4d, 8e	212.60	II
52.315	4c, 4d, 8f, 4b, 4a	93.126		133.469	8e, 8f	212.62	8b, 12d, 12c
52.316	8c, 8d, 8a, 8e	94.132	4b	133.470	8e	213.63	
52.317	4c, 4b, 4a, 4d	95.141	8c, 8b, 8a	134.480	8e	213.64	II
52.318	4c, 8d	95.142	4b, 4a, 8f	134.481	4c, 4d	213.66	12d, 12c, 8a
52.319	4b, 4a, 8d, 8h	96.144	II	134.482	8f	215.73	
52.320	4b, 4a, 4e	96.147	4a	135.484	II	216.77	
53.330	4c, 4a, 4f, 4e	96.148	4b, 4a, 8d	135.486	4c, 4a	218.82	II
53.331	4b, 4a, 8g	99.168		135.489	4c, 4b, 4a, 4d	219.86	II
53.332	4c, 4f, 4g, 4h, 4a, 4e	99.170		135.490		220.89	12a, 12b, 16c

TABLE VIII – *Continued from previous page*

MSGs	MWP	MSGs	MWP	MSGs	MWP	MSGs	MWP
53.333	4b, 4a, 4f, 4e	100.176	4a	135.491		220.90	II
53.335	4b, 4a, 8e	100.178	4a	135.492	4d	221.97	
53.336	4b, 4a, 4e	101.184	4c	135.494	4d, 4b	222.99	II
54.338	II	101.186		136.504		222.101	8c
54.342	4c, 4d, 4b, 4a, 4e	102.192		136.505	4a, 4e	222.102	
54.344	4c, 4d, 4b, 4a, 4e	102.193	4c, 4b	136.506	4c, 4d	223.105	II
54.345	4c, 4d, 4e	102.194	4b	137.508	II	223.108	
54.347	8c, 8d, 8a, 8e	103.196	II	137.510	8e	223.109	
54.348	4b, 4a, 4f, 4e	103.201	8c, 4a	137.511	8e	224.115	
54.349	8c, 8e	103.202	4a	137.514		225.121	
54.351	4b, 4a, 8h, 8c	104.204	II	137.516	8d	226.123	II
54.352	8c, 8d, 8a, 8e	104.208	4b, 4a	137.517	8e, 8f	226.126	
55.361	4c, 4a	104.209	4b, 8c	137.518	8f	227.133	96f
55.362	4b, 4a, 8e	105.216		138.520	II	228.135	II
55.364	4c, 4b, 4a, 4d	105.217	8c	138.522	4c, 4d	228.137	32b, 32c
56.366	II	105.218		138.524	4b, 4a	228.138	
56.369	4c, 4b, 4a, 4d	106.220	II	138.525	4c, 4d, 4b, 4a, 4e	230.145	24d, 16a
56.370	4c, 4b, 4a, 4d	106.224	4b	138.527	4e	230.146	II
56.371	4c, 4d	106.226	4b	138.528	4b, 8d	230.147	24c, 24d, 16b
56.372	8c, 8d, 8b, 8e	109.244	16b	138.530	8e	230.149	
56.373	4b, 4a, 8c						

TABLE IX: List of all single-valued magnetic space group (type I,II,III,IV) with 2-fold high symmetry planes, therefore all possible cases in magnons. The first column (MSGs) uses the BNS convention for the magnetic space group. The second (MWP) indicates the maximal Wyckoff position, if the magnon degenerate EBR is directly deducible from it (compatibility with magnetic order). If blank space then the degenerate EBR can only be induced in a composite magnon BR from a lower symmetric Wyckoff position. The type *II* group with pure time-reversal are also listed for completeness, signed with *II*, but they are not relevant for ordered magnonic systems with strong spin-orbit as considered in this paper.

MSGs	MWP	MSGs	MWP	MSGs	MWP	MSGs	MWP
3.5	2c, 2a, 2d, 2b	51.304	4b, 4a	64.471	8e	128.400	II
3.6	2a, 2b	52.306	II	64.472	8e	128.401	4d
4.8	II	52.307	4c, 4d	64.475	4b, 4a, 8e, 8c	128.402	4c
4.9	2a	52.309	4c, 4d	64.476	4b, 4a, 8e, 8c	128.405	4c, 4d, 2a, 2b
4.10	4a	52.310	4c, 4b, 4a, 4d	64.479	8c, 8e, 8b, 8f	128.406	
10.48	2c, 2g, 2a, 2d	52.311	4c, 4b, 4a, 4d	65.488	8e	128.408	4d, 4a
10.49	2c, 2a, 2d, 2b	52.314	4b, 4a, 8g	65.490	8e, 8f	128.410	4c, 2a, 2b
11.51	II	52.316	8c, 8d, 8a, 8e	66.498	4b, 4a, 8e	129.412	II
11.52	2e	52.317	4c, 4b, 4a, 4d	66.500	4b, 4a, 8e	129.413	
11.54	2d, 2a, 2b, 2c, 2e	52.318	4c, 8d	67.508	8c, 8e, 8b	129.414	4d, 4e
11.55	4c, 4a, 4e	52.319	4b, 4a, 8d, 8h	67.510	8c, 8d	129.417	4d, 2a, 2b, 2c, 4e
13.71	4d, 4a, 4f, 4e	52.320	4b, 4a, 4e	68.518	8c, 8e, 8g, 8a	129.418	
13.73	4f, 4e	53.322	II	68.520	8c, 8d, 8f	129.420	8d
13.74	4b, 4a, 4e	53.323	4g	75.4	4c, 2a, 2b	129.422	8f
14.76	II	53.324	4g	75.6	4b, 2a	130.424	II
14.77		53.327	2d, 4g, 2a, 2b, 2c	76.8	II	130.425	4c, 4a
14.79	2c, 2a, 2d, 2b	53.328	2d, 4g, 2a, 2b, 2c	76.11	8a	130.426	8d
14.80	4c, 4a	53.330	4c, 4a, 4f, 4e	77.16	4c	130.429	4c, 4b, 4a, 8d
14.82	4c, 4d, 4e	53.331	4b, 4a, 8g	77.18	4b	130.430	4b
16.4	2f, 2e, 2h, 2b	53.333	4b, 4a, 4f, 4e	78.20	II	130.432	4c, 4a, 8d
16.5	4k	53.334	2c, 2a, 2d, 2b	78.23	8a	130.434	4b, 4a, 8e
16.6		53.335	4b, 4a, 8e	81.36	2c, 4g, 2a	131.444	
17.8	II	53.336	4b, 4a, 4e	81.38	2a, 2b	131.445	8e
17.10	2c, 2a, 2d, 2b	54.338	II	83.48	2c, 2a, 4e	131.446	
17.11	4c, 4b, 4a, 4d	54.340	4c, 4d, 4e	83.50	4c, 2a, 2b	132.456	4f
17.13	2d, 4k, 2a, 2b, 2c	54.341	4c, 4d, 4e	84.56	4e	132.457	4b
17.14	4b, 4a	54.342	4c, 4d, 4b, 4a, 4e	84.58	4c, 4d	132.458	
17.15	4c, 4b, 4a	54.344	4c, 4d, 4b, 4a, 4e	85.64	4c, 4a, 8d	133.468	4d, 8e

TABLE IX – *Continued from previous page*

MSGs	MWP	MSGs	MWP	MSGs	MWP	MSGs	MWP
18.17	II	54.347	8c, 8d, 8a, 8e	85.66	4d, 8f	133.469	4b, 8e, 8f
18.18	2a, 2b	54.348	4b, 4a, 4f, 4e	86.72	4b, 8d	133.470	8e
18.19	2a, 2b	54.349	8c, 8e	86.74	8f	134.480	8e
18.20	4c, 4b, 4a, 4d	54.350	4g, 4f, 4b, 4a, 4e	89.92	2d, 4f, 2b	134.481	4c, 4d
18.21	4b, 4a	54.351	4b, 4a, 8h, 8c	89.93	4f, 4e	134.482	8f
18.22	4b, 4a	54.352	8c, 8d, 8a, 8e	89.94	4d	135.484	II
18.24	2c, 2a, 2d, 2b	55.354	II	90.96	II	135.485	4d
19.26	II	55.355		90.98	2c, 2a, 2b	135.486	4c, 4a
19.27	4a	55.356		90.99		135.489	4c, 4b, 4a, 4d
19.28	4b, 4a	55.357	2c, 2a, 2d, 2b	90.100	4c, 4b	135.490	4b
19.29	4b, 4a	55.358	2c, 2a, 2d, 2b	90.102	4c, 2a, 2b	135.492	4d
20.32	II	55.360	4c, 4d, 4f, 4e	91.104	II	135.494	4d, 4b
20.34	4b, 4a	55.361	4c, 4a	91.109	8c, 8b, 8a	136.496	II
20.36	8c, 8d, 8b, 8a	55.362	4b, 4a, 8e	91.110	4b, 4a, 8f	136.497	
21.42	4c, 4d, 8k	55.364	4c, 4b, 4a, 4d	92.112	II	136.498	4c
21.44	4c, 4d	56.366	II	92.114	4a	136.501	4c, 4d, 2a, 2b
25.61		56.367	4c, 4d	92.115	4a	136.502	4d
25.64		56.368	4c, 4d	92.116	4b, 4a, 8d	136.504	
25.65		56.369	4c, 4b, 4a, 4d	92.117	8c, 8b, 8a	136.506	4c, 4d
26.67	II	56.370	4c, 4b, 4a, 4d	93.124	4f	137.508	II
26.68	2a, 2b	56.372	8c, 8d, 8b, 8e	93.125	4c, 4b, 4d	137.509	
26.69	2a, 2b	56.373	4b, 4a, 8c	93.126		137.510	4d, 8e
26.71	4b, 4a	56.374	4b, 4a, 8e	94.128	II	137.513	4d, 8e, 2a, 2b
26.72	4b, 4a	56.376	4b, 4a, 8e	94.130	4d, 2a, 2b	137.514	
26.76	4a	57.378	II	94.131	4d	137.516	8d
27.82	2c, 2a, 2d, 2b	57.379	4c, 4d	94.132	4b	137.518	8f
27.85	4c, 4b, 4a	57.380	4c, 4d	94.134	4c, 4d	138.520	II
27.86	4b, 4a	57.381	4c, 4d	95.136	II	138.521	4a
28.94	4c, 4b, 4a	57.382	4c, 4b, 4a, 4d	95.141	8c, 8b, 8a	138.522	4c, 4d
28.95	4b, 4a	57.383	4c, 4b, 4a, 4d	95.142	4b, 4a, 8f	138.525	4c, 4d, 4b, 4a, 4e
28.96	4c, 4b, 4a	57.384	4c, 4b, 4a, 4d	96.144	II	138.526	4b, 4e
28.98	4b, 4a	57.386	8c, 8d, 8a	96.146	4a	138.528	4b, 8d
29.100	II	57.387	4c, 4d, 4f, 4e	96.147	4a	138.530	8e
29.101	4a	57.388	4d, 4b, 4f, 4e	96.148	4b, 4a, 8d	168.112	4b, 2a, 6c
29.102	4a	57.390	8c, 8e	96.149	8c, 8b, 8a	169.114	II
29.104	4b, 4a	57.391	4c, 8d	99.168		169.115	6a
29.105	8a	57.392	4b, 4a, 8e	99.170		170.118	II
29.109	4a	58.394	II	100.176	4a	170.119	6a
30.118	4c, 4b, 4a	58.395		100.178	4a	171.124	6b, 6a
30.119	2a, 2b	58.396		101.184	4c	172.128	6b, 6a
30.120	4a	58.397	2c, 2a, 2d, 2b	101.186		173.130	II
30.122	4b, 4a	58.398	2c, 2a, 2d, 2b	102.192		173.131	2a, 2b
31.124	II	58.400	4c, 4d, 8g	102.194	4b	175.142	4c, 2a, 6f
31.125	2a	58.401	4c, 4a	103.200	4c, 2a, 2b	176.144	II
31.126	2a	58.402	4c, 4b, 4a	103.202	4b, 4a	176.145	2c, 2a, 2d
31.128	4b, 4a	58.404	2c, 2a, 2d, 2b	104.208	4b, 4a	176.147	6g, 2b
31.129	4a	59.406	II	104.210	4b, 2a	177.154	4d, 6g, 2b
31.133	4a	59.407	2a, 2b	105.216		178.156	II
32.139	4b, 4a	59.408		105.218		178.157	6b, 6a

TABLE IX – *Continued from previous page*

MSGs	MWP	MSGs	MWP	MSGs	MWP	MSGs	MWP
32.142	4a	59.409	4c, 4d, 2a, 2b	106.224	4b	178.158	6b, 6a
32.143	4b, 4a	59.410	4c, 4d, 2a, 2b	106.226	4b	179.162	II
33.145	II	59.412	4d, 4b, 4f	111.256	4f	179.163	6b, 6a
33.146	4a	59.413	8c	111.257	4g	179.164	6b, 6a
33.147	4a	59.414	8d	111.258		180.172	6b, 6d
33.149	4a	59.416	8k	112.264	2d, 2a, 4e	181.178	6b, 6d
33.150	8a	60.418	II	112.265	4c, 8i	182.180	II
33.154	4a	60.419	4c	112.266	4d	182.181	2a
34.161	4b, 4a	60.420	4c	113.268	II	182.182	2c, 2d, 2b
34.162	4b, 4a	60.421	4c	113.269		183.190	
34.164	2a, 2b	60.422	4c, 4b, 4a	113.271	2c, 2a, 2b	184.196	4b, 2a, 6c
35.169	8c	60.423	4c, 4b, 4a	113.272	4a	185.198	II
35.171	8b	60.424	4c, 4b, 4a	113.274	4c, 4d	185.199	4b
36.173	II	60.426	8c, 8d, 8b, 8e	114.276	II	185.200	4b, 2a
36.174	4a	60.427	8c, 8d, 8a	114.277	4d	186.204	II
36.175	4a	60.428	4c, 4d, 8g	114.279	4d, 2a, 2b	186.205	2a, 2b
36.178	8b, 8a	60.429	8c, 8e	114.280	4c, 4b	186.206	
37.184	4b, 4a, 8c	60.431	4c, 4b, 4a	114.282	4c, 2a, 2b	191.242	
37.186	4a, 8b	60.432	4c, 4b, 4a, 4d	115.288		192.252	4c, 2a, 6f
47.254		61.434	II	115.290		193.254	II
47.255		61.435		116.296	2c, 4g, 2d	193.256	4c, 4d
47.256		61.436	4b, 4a	116.298	4d, 4b	193.257	4c, 2a
48.262	4b, 4a, 8e	61.438	8c, 8d, 8b	117.304	4d, 4a	193.258	6f
48.263	4f, 4e	61.439	4b, 4a, 8e	117.306	4b, 4a	193.259	4d, 6f, 2b
48.264	8k	62.442	II	118.312	4d, 4b	194.264	II
49.272	4c, 4a, 4f, 4h	62.443	4c	118.314	2c, 2d	194.266	2c, 2d, 2b
49.273	2f, 2e, 2a, 2b	62.444	4c	123.348		194.267	
49.274	4c, 4d, 4g	62.445	4c	123.349		194.268	6g, 2a
49.275	4c, 4d	62.446	4c, 4b, 4a	123.350		194.269	6g
49.276	4c, 4d	62.447	4c, 4b, 4a	124.360	2c, 4f, 2a	195.3	
50.284	4d, 4b, 4f, 4h	62.448	4c, 4b, 4a	124.361	4b, 8f	198.10	II
50.285	4c, 8e, 4d	62.450	4b, 4a, 8d	124.362	4c, 4d	200.17	
50.286	8d, 8h	62.451	4d, 4b	125.372	4b, 8e	201.21	8c
50.287	4f, 4e	62.452	8c, 8d, 8b	125.373	4f, 4e	205.34	II
50.288	8e	62.453	4c, 8d	125.374	8e	207.43	8c, 12d
51.290	II	62.454	4c, 4b, 4a	126.384	4c, 8e, 4a	208.47	
51.292	2f, 2e	62.455	8c, 8e	126.385	8e, 8f	212.60	II
51.293		63.458	II	126.386	4d, 8f	213.64	II
51.294	2d, 2a, 2b, 2f, 2c, 2e	63.459	4c	127.388	II	215.73	
51.296	2d, 2a, 2b, 2f, 2c, 2e	63.460		127.389		218.84	12d
51.299	4c, 4a, 4f	63.463	4c, 4b, 4a, 8d	127.390		221.97	
51.300	4b, 4a	63.464	4c, 4b, 4a, 8d	127.393	2c, 2a, 2d, 2b	222.103	8c, 12d
51.301	4b, 4a	63.467	8d, 8a, 8f	127.394		223.109	
51.302	4f, 4e	64.470	II	127.396	4a	224.115	
51.303	4b, 4a, 4f, 4e			127.398	4c, 4a		

TABLE X: List of magnetic space groups and relative Wyckoff positions which host a single decomposable EBR for spin waves. The column "MSGs" indicate the number of the space group in BNS setting, "MWP" the maximal Wyckoff position, "MPG" the magnetic point group isomorphic to the site symmetry group and finally "Bands" the number of bands composing the EBR. Total of 445 EBRs out of the 1907 single-valued ones.

MSGs	MWP	MPG	Bands	MSGs	MWP	MPG	Bands	MSGs	MWP	MPG	Bands
9.41	8a	1	4	89.92	4f	2'2'2	4	147.16	6e	-1	6
12.62	4e	-1	2	90.101	4e	2'2'2	4	148.17	9d	-1	3
12.62	4f	-1	2	90.101	4f	2'2'2	4	148.17	9e	-1	3
15.90	8f	-1	4	90.102	4c	2'2'2	4	148.20	18e	-1	6
15.91	8a	-1	4	91.109	8a	2	8	150.27	2d	3	2
15.91	8b	-1	4	91.109	8b	2'	8	150.28	4d	3	4
15.91	8e	2	4	92.116	8d	2'	8	157.55	2b	3	2
15.91	8f	2'	4	92.117	8a	2	8	159.64	4b	3	4
18.23	4k	2'	4	92.117	8b	2'	8	162.73	3f	2/m	3
20.35	8k	2'	4	92.117	8c	2'	8	162.73	3g	2/m	3
21.40	4k	2	2	92.118	8f	2'	8	162.77	2c	32'	2
21.41	4k	2'	2	94.129	4d	2	4	162.77	2d	32'	2
21.42	8k	2	4	94.130	4d	2	4	162.77	3f	2'/m'	3
23.52	8k	2'	4	94.133	4c	2'2'2	4	162.77	3g	2'/m'	3
24.56	8k	2	4	94.133	4d	2'2'2	4	162.78	6f	2/m	6
29.105	8a	1	8	94.133	4e	2'2'2	4	163.79	6g	-1	6
32.141	4c	2'	4	95.141	8a	2	8	163.83	6g	-1	6
35.167	4c	2'	2	95.141	8b	2'	8	163.84	4c	32'	4
35.168	4c	2	2	96.148	8d	2'	8	163.84	6f	2'/m'	6
36.177	8c	2'	4	96.149	8a	2	8	164.85	3e	2/m	3
36.179	8b	2'	4	96.149	8b	2'	8	164.85	3f	2/m	3
37.184	8c	2	4	96.149	8c	2'	8	164.89	2d	3m'	2
37.185	8a	2	4	96.150	8f	2'	8	164.89	3e	2'/m'	3
37.185	8b	2'	4	97.154	4c	2'2'2	2	164.89	3f	2'/m'	3
37.185	8c	2'	4	97.154	4d	2'2'2	2	164.90	6e	2/m	6
37.185	8d	2	4	97.156	8e	2'2'2	4	165.91	4d	3	4
37.186	8b	2	4	97.156	8f	2'2'2	4	165.91	6e	-1	6
41.217	8a	2	4	98.160	8f	2'	4	165.93	4d	3	4
41.217	8b	2'	4	98.162	8a	2'2'2	4	165.95	4d	3	4
41.217	8c	m'	4	98.162	8b	2'2'2	4	165.95	6e	-1	6
41.218	8b	2'	4	98.162	8c	2'2'2	4	165.96	4d	3m'	4
42.221	8b	2'	2	99.167	2c	m'm'2	2	165.96	6e	2'/m'	6
42.222	8b	2	2	100.177	4c	m'm'2'	4	166.97	9d	2/m	3
43.228	16a	2	4	101.182	4c	2	4	166.97	9e	2/m	3
43.228	16b	2'	4	101.183	4c	2	4	166.101	9d	2'/m'	3
45.239	8c	2'	4	102.190	4b	2	4	166.101	9e	2'/m'	3

TABLE X – *Continued from previous page*

MSGs	MWP	MPG	Bands	MSGs	MWP	MPG	Bands	MSGs	MWP	MPG	Bands
45.240	8a	2	4	102.191	4b	2	4	166.102	18e	2/m	6
45.240	8b	2'	4	103.195	4c	2	4	167.103	18d	-1	6
45.240	8c	m'	4	103.199	4c	2	4	167.107	18d	-1	6
48.262	8e	-1	8	103.200	4c	m'm'2	4	167.108	18e	2'/m'	6
48.264	8k	-1	8	103.201	8c	2'	8	168.109	2b	3	2
50.281	4e	-1	4	104.203	4b	2	4	168.109	3c	2	3
50.281	4f	-1	4	104.207	4b	2	4	168.111	3c	2'	3
50.286	8h	2'	8	104.209	8c	2'	8	168.112	4b	3	4
52.314	8g	2	8	104.210	4b	m'm'2	4	168.112	6c	2	6
52.315	8f	-1	8	105.217	8c	2'	8	173.132	6c	2'	6
52.318	8d	-1	8	106.219	4b	2	4	175.137	2c	-6	2
52.319	8d	-1	8	106.222	4a	2	4	175.137	2d	-6	2
52.319	8h	2	8	106.225	4a	m'm'2	4	175.137	3f	2/m	3
53.323	4g	2'	4	106.225	8c	2'	8	175.137	3g	2/m	3
53.325	4g	2'	4	107.231	4b	m'm'2	2	175.141	3f	2'/m'	3
53.326	4g	2'	4	108.238	8c	m'm'2'	4	175.141	3g	2'/m'	3
53.328	4g	2	4	109.244	16b	2'	8	175.142	4c	-6	4
54.347	8c	2	8	110.245	8a	2	4	175.142	6f	2/m	6
54.347	8e	2'	8	110.248	8a	2	4	176.143	6g	-1	6
56.373	8c	-1	8	110.250	8a	m'm'2	4	176.147	6g	-1	6
56.374	8e	2	8	110.250	16b	2'	8	176.148	6g	2'/m'	6
56.376	8e	-1	8	111.255	2e	2'2'2	2	177.151	3f	2'2'2	3
58.400	8g	2'	8	111.255	2f	2'2'2	2	177.151	3g	2'2'2	3
59.409	4c	-1	4	112.264	4e	2'2'2	4	177.152	3f	2'2'2	3
59.409	4d	-1	4	112.265	8i	2'	8	177.152	3g	2'2'2	3
60.426	8b	-1	8	113.273	4g	m'm'2'	4	177.153	2c	32'	2
60.426	8c	2'	8	114.275	4d	2	4	177.153	2d	32'	2
60.426	8d	2'	8	114.277	4d	2	4	177.153	3f	2'2'2	3
60.426	8e	2	8	114.279	4d	2	4	177.153	3g	2'2'2	3
60.428	8g	2'	8	114.281	8i	2'	8	177.154	4d	32'	4
60.429	8c	-1	8	114.282	4c	2'2'2	4	177.154	6g	2'2'2	6
60.429	8e	2'	8	115.287	2g	m'm'2	2	182.184	6f	2'2'2	6
60.430	8c	-1	8	116.291	4i	2	4	182.184	6g	2'2'2	6
60.430	8h	2'	8	116.294	4i	2	4	183.187	3c	m'm'2'	3
61.438	8b	-1	8	116.295	4i	2	4	183.188	3c	m'm'2'	3
61.438	8c	2'	8	116.296	4g	m'm'2	4	183.189	2b	3m'	2
61.438	8d	m'	8	117.305	4e	2'2'2	4	183.189	3c	m'm'2	3
61.439	8e	2'	8	117.305	4f	2'2'2	4	184.191	4b	3	4
61.440	8b	-1	8	120.326	8e	2'2'2	4	184.191	6c	2	6
61.440	8c	2'	8	120.326	8f	2'2'2	4	184.193	6c	2'	6
61.440	8d	2'	8	121.331	4c	2'2'2	2	184.194	6c	2'	6
61.440	8e	2'	8	121.331	4d	-4	2	184.195	4b	3	4
62.455	8e	2'	8	121.332	8g	m'm'2'	4	184.195	6c	2	6
63.462	8d	-1	4	122.335	8d	2'	4	184.196	4b	3m'	4
63.464	8d	-1	4	122.337	8d	2'	4	184.196	6c	m'm'2	6
64.471	8e	2'	4	123.345	2e	m'm'm	2	185.200	4b	3	4
64.473	8e	2'	4	123.345	2f	m'm'm	2	185.201	4b	3	4
64.474	8c	-1	4	124.351	4e	2/m	4	185.202	6c	m'm'2'	6

TABLE X – *Continued from previous page*

MSGs	MWP	MPG	Bands	MSGs	MWP	MPG	Bands	MSGs	MWP	MPG	Bands
64.474	8e	2'	4	124.353	4f	2'2'2	4	186.208	6c	m'm2'	6
64.475	8e	2'	4	124.357	4e	2/m	4	189.225	2c	-6	2
64.476	8c	-1	4	124.357	4f	2'2'2	4	189.225	2d	-6	2
64.476	8e	2	4	124.360	4f	m'm'm	4	190.232	4d	-6	4
64.477	8e	2	4	125.369	4e	2'/m'	4	191.238	3f	m'm'm	3
65.485	4e	2/m	2	125.369	4f	2'/m'	4	191.238	3g	m'm'm	3
65.485	4f	2/m	2	126.375	8f	-1	8	191.239	3f	m'm'm	3
66.498	8e	2/m	4	126.377	4c	2'2'2	4	191.239	3g	m'm'm	3
66.500	8e	2/m	4	126.381	4c	2'2'2	4	191.240	2c	-6m'2'	2
68.513	8h	2'	4	126.381	8f	-1	8	191.240	2d	-6m'2'	2
68.514	8h	2	4	126.384	8e	2'/m'	8	191.240	3f	m'm'm	3
68.515	8h	2	4	126.385	8f	2'2'2	8	191.240	3g	m'm'm	3
68.516	8c	-1	4	126.386	8f	2'/m'	8	192.243	4d	-6	4
68.516	8d	-1	4	128.399	4c	2/m	4	192.243	6g	2/m	6
68.516	8h	2'	4	128.401	4d	2'2'2	4	192.245	4c	32'	4
68.517	8h	2	4	128.405	4c	2/m	4	192.245	6f	2'2'2	6
68.519	8f	2'2'2	4	128.409	8f	2'2'2	8	192.246	6f	2'2'2	6
68.519	8g	2'2'2	4	128.410	4c	m'm'm	4	192.247	6f	2'2'2	6
69.524	8e	2/m	2	129.417	4d	2'/m'	4	192.248	6f	2'2'2	6
69.524	8f	2'2'2	2	129.417	4e	2'/m'	4	192.248	6g	2'/m'	6
70.532	16b	2'2'2	4	130.423	8d	-1	8	192.249	6f	2'2'2	6
70.532	16c	2'2'2	4	130.429	8d	-1	8	192.249	6g	2'/m'	6
70.532	16d	2'2'2	4	130.432	8d	2'/m'	8	192.250	4c	32'	4
70.532	32e	-1	8	130.433	8f	2'2'2	8	192.250	4d	-6	4
71.536	8k	-1	4	130.434	8e	2'/m'	8	192.250	6f	2'2'2	6
72.543	8e	-1	4	132.451	4f	2/m	4	192.250	6g	2/m	6
72.544	8e	-1	4	132.453	4e	2'2'2	4	192.252	4c	-6m'2'	4
73.550	8c	2	4	132.453	4f	2/m	4	192.252	6f	m'm'm	6
73.550	8d	2'	4	132.454	4e	2'2'2	4	193.253	6f	2/m	6
73.550	8e	2'	4	133.461	4b	2'2'2	4	193.257	4c	-6	4
75.1	2c	2	2	133.462	8e	-1	8	193.258	6f	2/m	6
75.4	4c	2	4	133.465	8e	-1	8	193.259	4d	32'	4
75.5	4c	2'	4	133.466	4a	2'2'2	4	193.259	6f	2'/m'	6
75.6	4b	2	4	133.469	8e	2'2'2	8	193.260	4c	-6	4
76.11	8a	1	8	134.477	4c	2'2'2	4	193.260	4d	32'	4
77.17	4a	2	4	134.477	4d	2'2'2	4	193.260	6f	2'/m'	6
77.17	4b	2	4	134.478	4c	2'2'2	4	193.262	6g	m'm'm	6
77.17	4c	2'	4	135.485	4d	2'2'2	4	194.263	6g	2/m	6
78.23	8a	1	8	135.493	8e	2'2'2	8	194.268	6g	2'/m'	6
79.25	4b	2	2	136.499	4c	2/m	4	194.269	6g	2/m	6
79.28	8c	2'	4	136.501	4c	2/m	4	194.270	6g	2'/m'	6
80.32	8a	2'	4	137.510	8e	-1	8	194.272	6g	m'm'm	6
80.32	8b	2'	4	137.512	4d	m'm'2	4	198.11	12b	2'	12
80.32	8c	2	4	137.513	4d	m'm'2	4	203.29	48d	2'2'2	12
81.33	2g	2	2	137.513	8e	-1	8	205.36	24d	2'	24
81.36	4g	2	4	137.517	8e	2'2'2	8	206.37	24d	2	12
81.37	4g	2'	4	139.537	4c	m'm'm	2	207.43	12d	2'2'2	12
82.42	8g	2'	4	139.537	8f	2'/m'	4	210.55	32c	32'	8

TABLE X – *Continued from previous page*

MSGs	MWP	MPG	Bands	MSGs	MWP	MPG	Bands	MSGs	MWP	MPG	Bands
83.43	2e	2/m	2	140.547	8e	2'/m'	4	210.55	48d	2'2'2	12
83.43	2f	2/m	2	141.560	16c	2'2'2	8	210.55	48e	2'2'2	12
83.48	4e	2/m	4	142.563	8b	2'2'2	4	210.55	48f	2'2'2	12
83.50	4c	2/m	4	142.563	16e	2'	8	211.58	8c	32'	4
85.59	4d	-1	4	142.564	16c	-1	8	211.58	12d	2'2'2	6
85.59	4e	-1	4	142.564	16e	2'	8	212.62	12c	2'2'2	12
85.64	8d	-1	8	142.566	16e	2	8	212.62	12d	2'2'2	12
85.66	8f	-1	8	142.567	16c	-1	8	213.66	12c	2'2'2	12
86.67	4e	2	4	142.567	16e	2'	8	213.66	12d	2'2'2	12
86.70	4e	2	4	142.568	16e	2'	8	218.84	12d	-4	12
86.71	4e	2	4	142.569	16e	2	8	222.98	12d	-4	12
87.75	4c	2/m	2	142.570	16c	2'2'2	8	222.103	12d	-42'm'	12
87.75	8f	-1	4	147.13	2d	3	2	223.106	8e	32'	8
88.86	16c	-1	8	147.13	3e	-1	3	224.113	12f	2'2'2	12
88.86	16e	2'	8	147.13	3f	-1	3	227.133	96f	2'2'2	24
89.90	2e	2'2'2	2	147.16	4d	3	4	228.139	96f	2'2'2	24
89.90	2f	2'2'2	2								